Quantum phase diagram of the integrable p_x+ip_y fermionic superfluid

Stefan M. A. Rombouts* and Jorge Dukelsky
Instituto de Estructura de la Materia, CSIC, Serrano 123, E-28006 Madrid, Spain

Gerardo Ortiz
Department of Physics, Indiana University, Bloomington, Indiana 47405, USA
(Received 26 August 2010; published 13 December 2010)

We determine the zero-temperature quantum phase diagram of a p_x+ip_y pairing model based on the exactly solvable hyperbolic Richardson-Gaudin model. We present analytical and large-scale numerical results for this model. In the continuum limit, the exact solution exhibits a third-order quantum phase transition, separating a strong-pairing from a weak-pairing phase. The mean-field solution allows to connect these results to other models with p_x+ip_y pairing order. We define an experimentally accessible characteristic length scale, associated with the size of the Cooper pairs, that diverges at the transition point, indicating that the phase transition is of a confinement-deconfinement type without local order parameter. We propose an experimental measurement to detect the transition. We show that this phase transition is not limited to the p_x+ip_y pairing model but can be found in any representation of the hyperbolic Richardson-Gaudin model and is related to a symmetry that is absent in the rational Richardson-Gaudin model.

DOI: 10.1103/PhysRevB.82.224510 PACS number(s): 74.20.Fg, 74.20.Rp, 71.10.Hf, 73.43.Nq

I. INTRODUCTION

One of the striking features of degenerate Fermi gases whose constituents interact through an attractive potential is that they can exhibit superfluidity or superconductivity. The constituents may be neutral atoms, as is the case in trapped Fermi gases of ^{40}K and ^{6}Li (Ref. 1) or superfluid ^{3}He,[2] or charged electrons as in conventional metallic superconductors, nucleons in heavy nuclei or nuclear matter.[3] The particular nature and symmetry of the attractive pairing interaction may lead to exotic superfluid phases with complex order parameters, as is well known in the case of liquid ^{3}He. For order parameters with certain rotational symmetries, a change in the coupling strength may induce a quantum phase transition (QPT) separating different kinds of superfluid phases. In a Fermi system whose pairing interaction has an s-wave character, it is well understood that by increasing the coupling strength there is a crossover, and not a QPT, between a weak-coupling Bardeen-Cooper-Schrieffer[4] (BCS) and a Bose-Einstein condensate (BEC) phase.[5] However, for higher rotational order, the ground state can exhibit a QPT between qualitatively different superfluid states, with a corresponding nonanalyticity in the ground-state energy. In the present paper we focus on p-wave pairing that might be encountered in ultracold Fermi gases[6–12] or in exotic superconductors such as Sr_2RuO_4.[13]

As a schematic model for such systems we study the quantum phase diagram of a spinless Fermi gas with p_x+ip_y pairing interaction symmetry

$$H_{p_x+ip_y}=\sum_k \frac{k^2}{2}c_k^\dagger c_k-\sum_{k,k'}V_{kk'}c_k^\dagger c_{-k}^\dagger c_{-k'}c_{k'}, \tag{1}$$

where $V_{kk'}=g_k^*g_{k'}$ is a separable interaction, with g_k representing a complex function of wave vector k and symmetry p_x+ip_y. Though schematic, this model captures the basic physics of the BEC and BCS sides of the phase diagram and offers detailed insights into the phase-transition mechanism. Previous studies concentrated on the standard mean-field description.[14–17] The interesting point of the Hamiltonian in Eq. (1) is that under certain conditions on the pairing coefficients g_k the model is integrable and can be solved exactly with a Bethe ansatz.[18] This has the important consequence that it demonstrates that the BEC-BCS QPT in this model is not an artifact of the mean-field approximation, even though the ground-state few-points correlation functions and energy density coincides with the mean-field ones in the thermodynamic limit for attractive interactions. Furthermore, the defining properties of the Bethe ansatz wave function are so qualitatively distinct from its mean-field counterpart that it deserves further investigation. Indeed, as we will see, some features and insights resulting from the Bethe ansatz state are absent in the mean-field solution.

In this paper we restrict specific calculations to the two-dimensional attractive case where a QPT with unusual characteristics signals the transition between two gapped superfluid phases, one topologically nontrivial, known as weak pairing,[19] and another one characterized by tightly bound quasimolecules, known as strong pairing.[14] The quantum phase diagram of the two-dimensional p_x+ip_y spinless fermion pairing Hamiltonian displays several peculiarities (see Fig. 1), depending on the fermion density ρ. For dense gases, $\rho>1/2$, there is no QPT of any sort. When $\rho<1/2$, the model displays a QPT between weak-pairing and strong-pairing phases while otherwise the ground-state energy is an analytic function of the coupling strength g. Volovik anticipated,[20] using an equivalent effective field theory, that a QPT of this kind can be signaled by a discontinuous change in a topological quantum number. We show that the transition is continuous and *third order* (meaning that the third-order derivative of the ground-state energy is discontinuous), contrary to what has been claimed in the literature.[21,22] Furthermore, we demonstrate that this phase transition can be related to an experimentally accessible length scale that diverges logarithmically at the phase-transition point. We give an interpretation of this length scale in terms of the size of

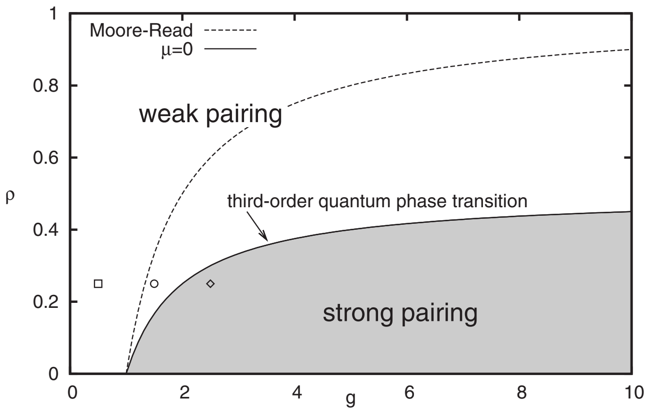

FIG. 1. Quantum phase diagram of the p_x+ip_y or hyperbolic model in terms of the fermion density ρ and the attractive coupling strength g. It shows two superfluid phases, strong-pairing (confined) and weak-pairing (deconfined) phases, separated by a third-order confinement-deconfinement QPT at vanishing chemical potential, $\mu=0$. Cooper pairs deconfine between the phase-transition line and the Moore-Read line (indicated by a dashed line). The latter line corresponds to $\rho=1-1/g$ and vanishing total energy, $E=0$, and represents a situation where all Cooper pairs are deconfined. The small symbols at $\rho=0.25$ (quarter filling) indicate the configurations that are displayed in detail in Figs. 3 and 4.

the Cooper pairs, with strong pairing corresponding to confined pairs that start to deconfine when the system enters the weak-pairing phase, and that eventually convert to plane waves in the weakly interacting limit.

A peculiar boundary in the quantum phase diagram is the so-called Moore-Read line[23] (shown as a dashed line in Fig. 1). The latter separates in principle a weak-coupling BCS regime from the weak-pairing phase and is defined for a particular relation between the density ρ and the interaction strength g: $\rho=1-1/g$. At this line all Cooper pairs become deconfined. As explained in detail in the text, our calculations indicate that there is no QPT at the Moore-Read line, contrary to what is advocated in Refs. 18 and 22. Thus, the weak-coupling BCS region and the weak-pairing phase are adiabatically connected.

Technically, we solve the more general hyperbolic (or XXZ) Richardson-Gaudin (RG) model first introduced in Refs. 24 and 25, and recently realized to be related to the p_x+ip_y two-dimensional superfluid.[18] We present results for finite systems and, for determining the quantum phase diagram, the relevant thermodynamic limit. Calculating those results for the hyperbolic RG model implies solving the corresponding Bethe ansatz equations, a task that may happen to be technically challenging, specifically for large finite systems. Here, we introduce a technique that solves the Bethe ansatz equations numerically in polynomial time. For very large systems one can define a thermodynamic limit that allows one to solve the equations for the integrable p_x+ip_y model analytically.[22]

We want to emphasize that *any* hyperbolic RG model in the continuum limit displays the nonanalytic behavior observed at the equivalent $\mu=0$ line as long as the parameters defining the model vanish at a given zero mode (e.g., $k=0$ mode). The underlying algebraic structure of the hyperbolic RG model allows us to prove a theorem that relates subspaces with different number of pairs but with the same eigenvalues, thereby generalizing a relation from Ref. 18 to all representations of the hyperbolic RG model. These relations are inexistent in the case of the rational RG model (e.g., the s-wave BCS superconductor) and are indeed at the root of the existence of the QPT between the weak- and strong-pairing phases.

In Sec. II we discuss the algebraic properties of the hyperbolic RG model. In Sec. III we present numerical and analytical results for the p_x+ip_y model, analyze the phase diagram, and interpret the QPT mechanism. Using an affine Lie algebra, we show in Sec. IV that the hyperbolic RG model possesses a symmetry that relates the two phases. In the Appendices we give a detailed solution of the hyperbolic RG model for one pair (Appendix A), for one level (Appendix B), in the continuum limit (Appendix C), and in the mean-field approximation (Appendix D).

II. ALGEBRAIC FORMULATION OF THE INTEGRABLE p_x+ip_y MODEL AND ITS SOLUTIONS

A. Generalized Gaudin algebra

The p_x+ip_y integrable pairing model can be obtained as a particular parametrization of the exactly solvable hyperbolic family derived from the generalized Gaudin algebra. We recapitulate here the main ingredients of the procedure to construct such exactly solvable models that we have laid out in previous work.[26] At the same time, this serves to demonstrate that particular features of the zero-temperature phase diagram of the p_x+ip_y model are not limited to this representation and analogs can be found in many other representations of the same underlying Gaudin algebra. Assuming a system characterized by l levels (representations) of an $su(2)$ algebra labeled by the (in principle arbitrary) quantum number i, the generic form of the exactly solvable RG Hamiltonians is

$$H=\sum_i \epsilon_i S_i^z-\sum_{i,j}(\epsilon_i-\epsilon_j)X(\eta_i,\eta_j)S_i^+S_j^- \\ -\sum_{i,j}(\epsilon_i-\epsilon_j)Z(\eta_i,\eta_j)S_i^zS_j^z, \tag{2}$$

where the operators S_i^+, S_i^-, and S_i^z close the $su(2)$ commutator algebra, and $X(x,y)$ and $Z(x,y)$ are antisymmetric functions depending on l parameters η_i to be determined later on. The generic Hamiltonian (2) commutes with the squared spin operator of each level, $\mathbf{S}_i^2=S_i^z(S_i^z-1)+S_i^+S_i^-$, and with the total spin operator $\mathbf{S}=\Sigma_i\mathbf{S}_i$. Let us introduce the notation s_i for the spin value of level i, such that $\langle\mathbf{S}_i^2\rangle=s_i(s_i+1)$. Apart from this, one can evaluate the commutator between two such Hamiltonians, H and H', based on the same set of parameters η_i but with distinct sets of parameters ϵ_i and ϵ_i'. It turns out that H and H' commute provided that the functions $X(x,y)$ and $Z(x,y)$ fulfill the following condition for all x, y, and z known as the Gaudin condition[27]

$$[Z(x,y)-Z(x,z)]X(y,z)-X(x,y)X(x,z)=0. \tag{3}$$

A consequence of this condition is that

$$X(x,y)^2 - Z(x,y)^2 = \Gamma, \tag{4}$$

where Γ is a constant independent of x and y. Then, by a suitable choice of the parameters ϵ_i in Eq. (2), one can define a set of l linearly independent constants of motion, which commute among themselves

$$R_i = S_i^z - \sum_{j,j\neq i} X(\eta_i,\eta_j)(S_i^+ S_j^- + S_i^- S_j^+) - 2\sum_{j,j\neq i} Z(\eta_i,\eta_j) S_i^z S_j^z. \tag{5}$$

Therefore, Hamiltonians of the form of Eq. (2) are integrable,[26] and furthermore, they can be solved exactly by a Bethe ansatz.

It is convenient to define the following operators:

$$\mathsf{S}^z(x) = -\frac{1}{2} - \sum_j Z(x,\eta_j) S_j^z, \quad \mathsf{S}^\pm(x) = \sum_j X(x,\eta_j) S_j^\pm. \tag{6}$$

They fulfill the commutation relations of an *XXZ Gaudin algebra*,

$$[\mathsf{S}^z(x),\mathsf{S}^\pm(y)] = \pm[X(x,y)\mathsf{S}^\pm(x) - Z(x,y)\mathsf{S}^z(y)],$$

$$[\mathsf{S}^+(x),\mathsf{S}^-(y)] = 2X(x,y)[\mathsf{S}^z(x) - \mathsf{S}^z(y)]. \tag{7}$$

With this notation, the Bethe ansatz for the eigenstates of order M takes the form

$$|\Phi_M\rangle = \left[\prod_{\alpha=1}^{M} \mathsf{S}^+(E_\alpha)\right]|\nu\rangle, \tag{8}$$

where $|\nu\rangle$ is a vacuum state such that $S_i^-|\nu\rangle=0$, and $S_i^z|\nu\rangle = -s_i|\nu\rangle$ for all i. The unknowns E_α are solutions of a set of nonlinear equations, the RG equations

$$\sum_i s_i Z(\eta_i,E_\alpha) - \sum_{\alpha',\alpha'\neq\alpha} Z(E_{\alpha'},E_\alpha) = \frac{1}{2}, \quad \forall \quad \alpha. \tag{9}$$

We will call the variables E_α *pairons*.[28] Equation (9) does not depend on the parameters ϵ_i, which means that the eigenstates given by Eq. (8) do not depend on these parameters either. This is due to the fact that the ansatz from Eq. (8) represents the eigenstates of the complete set of the integrals of motion R_i, and therefore of any linear combination of R_i's, as given by Hamiltonian (2) whose eigenvalues are given by

$$E(\Phi_M) = \langle\nu|H|\nu\rangle + 2\sum_{i,\alpha} s_i\epsilon_i Z(\eta_i,E_\alpha). \tag{10}$$

For $\Gamma=0$ one recovers the *rational* RG model, that can be parametrized as

$$X(x,y) = Z(x,y) = \frac{G}{x-y} \tag{11}$$

[any other expression for X and Z that fulfills Eqs. (3) and (4) at $\Gamma=0$ can be transformed to this form through a redefinition of parameters]. In this work we will focus on the properties of the *hyperbolic* RG model, which correspond to $\Gamma<0$. Any set of functions $X(x,y)$ and $Z(x,y)$ that fulfills Eqs. (3) and (4) with $\Gamma=-\gamma^2$, can be mapped onto the following parametrization:[26]

$$X(x,y) = 2\gamma\frac{\sqrt{x}\sqrt{y}}{x-y}, \quad Z(x,y) = \gamma\frac{x+y}{x-y}. \tag{12}$$

We can simplify the discussion by choosing $\epsilon_i=\lambda\eta_i$, with λ a parameter that will be fixed later on. Using this parametrization, and subtracting a diagonal term $2\gamma\Sigma_i\eta_i\mathbf{S}_i^2$, one obtains an interesting form for the Hamiltonian of Eq. (2),

$$\begin{aligned} H &= \lambda(1+2\gamma)\sum_i \eta_i S_i^z - \lambda\gamma\sum_{i,j}(\eta_i+\eta_j)S_i^z S_j^z \\ &\quad - 2\lambda\gamma\sum_{i,j}\sqrt{\eta_i\eta_j}S_i^+S_j^- \\ &= \lambda(1+2\gamma-2\gamma S^z)\sum_i \eta_i S_i^z - 2\lambda\gamma\sum_{i,j}\sqrt{\eta_i\eta_j}S_i^+S_j^-. \end{aligned} \tag{13}$$

Now we can take advantage of the fact that $S^z=\Sigma_i S_i^z$ is a constant of motion,

$$S^z|\Phi_M\rangle = (M-L/2)|\Phi_M\rangle, \tag{14}$$

where $L=2\Sigma_i s_i$ is the maximum value that the model allows for the order M (therefore L is a useful measure for the dimension of the model space; e.g., if $s_i=1/2$ for all levels, then L equals the number of levels l). This allows us to fix the parameters λ and γ such that

$$\lambda[1+\gamma(L-2M+2)] = 1, \quad 2\lambda\gamma = G, \tag{15}$$

leading to a separable Hamiltonian for the hyperbolic RG model

$$H_h = \sum_i \eta_i S_i^z - G\sum_{i,j}\sqrt{\eta_i\eta_j}S_i^+S_j^-. \tag{16}$$

The corresponding RG equations, Eq. (9), reduce to

$$\sum_i \frac{s_i}{\eta_i - E_\alpha} - \sum_{\alpha',\alpha'\neq\alpha}\frac{1}{E_{\alpha'}-E_\alpha} - \frac{Q}{E_\alpha} = 0, \quad \forall \quad \alpha \tag{17}$$

with

$$Q = \frac{1}{2G} - \frac{L}{2} + M - 1. \tag{18}$$

The eigenstates of H_h, $|\Phi_M\rangle$ of Eq. (8), involve the pair operator

$$\mathsf{S}^+(E_\alpha) = \sum_i \frac{\sqrt{\eta_i}}{\eta_i - E_\alpha} S_i^+, \tag{19}$$

defined in terms of the spectral parameters E_α obtained from Eq. (17), and have energy eigenvalues given by Eq. (10),

$$E(\Phi_M) = \langle\nu|H_h|\nu\rangle + \sum_\alpha E_\alpha. \tag{20}$$

For the remaining discussion we will assume that $\langle\nu|H_h|\nu\rangle = 0$, which amounts to a simple shift in the energy scale, without loss of generality.

In the pairing representations each $su(2)$ copy is associated with a single-particle level i. M is the number of active pairs. The vacuum $|\nu\rangle$ is now defined by a set of seniorities, $|\nu\rangle=|\nu_1,\nu_2,\ldots,\nu_l\rangle$, where the *seniority* ν_i is the number of unpaired particles in level i with single-particle degeneracy Ω_i, such that $s_i=(\Omega_i-2\nu_i)/4$.

In two spatial dimensions, one can define a representation of the $su(2)$ algebra in terms of spinless fermions in momentum space, $c_k^\dagger$, c_k. One obtains a level η_k for each pair of states $(k,-k)$, where the index k now refers to the momentum in two dimensions (in order to avoid double counting we select $k_x>0$ to label the levels). Furthermore, one can include a phase factor in the definition of $\mathbf{S}_k$,

$$S_k^z=\frac{1}{2}(c_k^\dagger c_k+c_{-k}^\dagger c_{-k}-1),\qquad S_k^+=\frac{k_x+ik_y}{|k|}c_k^\dagger c_{-k}^\dagger,$$
$$S_k^-=\frac{k_x-ik_y}{|k|}c_{-k}c_k. \tag{21}$$

By taking $\eta_k=k^2$, one obtains the p_x+ip_y model presented by Ibañez *et al.*[18]

$$H_{p_x+ip_y}=\sum_{k,k_x>0}\frac{k^2}{2}(c_k^\dagger c_k+c_{-k}^\dagger c_{-k}) - G\sum_{\substack{k,k_x>0,\\ k',k'_x>0}}(k_x+ik_y)(k'_x-ik'_y)c_k^\dagger c_{-k}^\dagger c_{-k'}c_{k'}. \tag{22}$$

In the case of cold atom gases, the spinless fermions operators represent atoms in the same hyperfine state.

It is important to emphasize that Hamiltonian $H_{p_x+ip_y}$ has an $SU(2)$ gauge symmetry.[29] The $SU(2)$ symmetry generators are the local operators

$$\tau_k^+=c_k^\dagger c_{-k}=(\tau_k^-)^\dagger,\qquad \tau_k^z=\frac{1}{2}(c_k^\dagger c_k-c_{-k}^\dagger c_{-k}), \tag{23}$$

which commute with the $su(2)$ algebra generators of Eq. (21). This local symmetry amounts to the conservation of the charge parity per mode pair $(k,-k)$, and is responsible for the Pauli blocking of the (unpair) singly occupied states.

B. Singularities in the Richardson-Gaudin equations

Just like in the rational case, the RG equations become singular when two or more pairons approach the same level.[30,31] Analyzing the residues in the equation, one finds that the number of singular pairons has to be equal to $2s_k+1$ for a singularity around level η_k. However, around $E_\alpha=0$, Eq. (17) for the hyperbolic RG model displays a peculiar singularity not present in the rational models. Let us analyze what happens when N of the pairons converge to zero energy, and $M-N$ pairons do not. For the pairons that do not converge to zero, one finds that the equations correspond to a state of order $M-N$ with all pairons distinct from zero. In the equations for the N singular pairons the contributions of the nonsingular pairons and the levels η_k are of order one and become negligible compared to the singular terms. Therefore we can replace the nonsingular terms by a single level, with an averaged level parameter η given by

$$\frac{L/2-(M-N)}{\eta}=\sum_k\frac{s_k}{\eta_k}-\sum_{\alpha',E_{\alpha'}\nrightarrow 0}\frac{1}{E_{\alpha'}}. \tag{24}$$

Appendix B gives the analytical solution of the one-level problem. One finds that a necessary condition to have N values converging to zero is that $2Q+1=N$, or

$$\frac{1}{G}=L-2M+N+1. \tag{25}$$

We recognize two special cases: *special case (i)* $N=0$. No pairons can converge to zero for $\frac{1}{G}\leq L-2M+1$; we will see that this boundary coincides with the phase-transition line in Fig. 1. *Special case (ii)* $N=M$. All pairons can converge to zero for $\frac{1}{G}=L-M+1$; this situation determines the so-called *Moore-Read* line[18,23] in Fig. 1. Between these two regimes, a fraction of the pairons can converge to zero at integer values of G^{-1}.

To obtain a qualitative view of the quantum phase diagram of Fig. 1, we will interpret the pair wave functions resulting from $\mathsf{S}^+(E_\alpha)$ in Eq. (19) as scattering states if the pairon E_α is real and positive, as a Cooper resonance if E_α is complex, and as a bound pair state if E_α is real and negative. Although the total wave function is an eigenstate of the Hamiltonian (i.e., a stationary state), the meaning of *resonance* or *bound* pair states results from considering each pair as isolated. The pair resonance (complex pairon) is not a decaying state but it will acquire a finite lifetime if a physical process could isolate it from the rest of the system. Analogously, a pair with a real and negative pairon that is suddenly isolated would behave as a highly excited dimer. On the left side of the phase diagram one finds the weak coupling BCS region, where the pairons behave much like in the rational model: a fraction of the pairons form an arc in the complex plane defining a set of Cooper pair resonance while the rest of the pairs with real and positive pairons are scattering states. If the coupling strength is increased, one reaches the Moore-Read line that coincides with special case (ii) where all pairons collapse to zero. Increasing the interaction strength, still in weak pairing, some of the pairons can collapse to zero (at integer values of G^{-1}) while the others are real and negative. We therefore, interpret this region as a mixture of Cooper resonances and bound molecular states. Finally, for strong interactions and $M<L/2$, the system makes a transition to the strong-pairing phase. Here the ground state corresponds to a configuration where all pairons are real and negative, i.e., a BEC of bound molecular states.

At the Moore-Read line all pairons E_α converge to zero, which means that the total energy E also goes to zero. This coincides exactly with the mean-field result. The corresponding wave functions are not the same because the mean-field wave function breaks pair number symmetry, and can be written as a superposition of exact zero-energy states for a range of numbers of pairs

$$|\psi_{\mathsf{mf}}\rangle\propto\exp\left(\Delta\sum_{k,k_x>0}\frac{1}{k_x-ik_y}c_k^\dagger c_{-k}^\dagger\right)|\nu\rangle \tag{26}$$

while the exact wave function is given by the projection of $|\psi_{\mathsf{mf}}\rangle$ onto the M-pair sector,

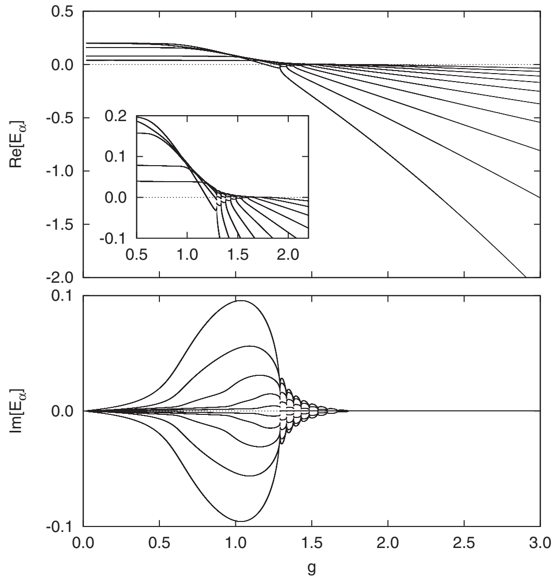

FIG. 2. Real and imaginary parts of the spectral parameters E_α as a function of $g=GL$ for ten pairons in a disk of dimension $L=40$ (quarter filling), with levels as specified in Table I.

$$|\psi_M\rangle \propto \left(\sum_{k,k_x>0} \frac{1}{k_x - ik_y} c_k^\dagger c_{-k}^\dagger\right)^M |\nu\rangle. \tag{27}$$

Just below the line, when $N=M-1=L-1/G-1$, one finds that the energy of the exact eigenstate is equal to the energy E_p of the one-pair state calculated in Appendix A because of the symmetry to be shown in Sec. IV. Increasing the number of pairs by one while maintaining G fixed, moves the state to the Moore-Read line where the total energy is zero. This means that for a small increase in density, $\Delta M/L=1/L$ (which becomes infinitesimal in the thermodynamic limit), there is a finite jump in energy, $\Delta E=|E_p|$. This is interpreted by Ibañez *et al.* as a signature of a *zeroth-order QPT*. Note however, that E scales proportional to ωL, where ω is the kinetic-energy cutoff as defined in Appendix A. Therefore, the shift in energy ΔE resulting from a shift in density $\Delta M/L$ is given by

$$\Delta E = \frac{dE}{dM}\Delta M = \omega \frac{dE/(\omega L)}{d(M/L)}\Delta M, \tag{28}$$

which is of order ω for $\Delta M=1$ because the derivative is free of scales. This means that a jump in energy of size $|E_p|$ for a change in density of size $1/L$ is not a sign of a phase transition but rather a consequence of the pathological scaling behavior of the energy in this model.

III. QUANTUM PHASE DIAGRAM OF THE INTEGRABLE p_x+ip_y MODEL

A. Case of finite systems

We would like to stress here that in order to obtain the exact solution of the pairing eigenproblem for M pairs in a system of size L, one has to diagonalize a Hamiltonian matrix of dimension $L!/(M!(M-L)!)$. The integrability of the RG model reduces the exponential complexity of the problem to that of solving a set of M nonlinear equations in M unknowns, Eq. (17), which can be done in polynomial time. This justifies labeling these models as *exactly solvable*. For instance, below we show exact results for $L=504$ and $M=126$, which corresponds to solving an eigenvalue problem of dimension 10^{122} while in our case each eigenvector arises as a particular solution of the 126 coupled nonlinear RG equations.

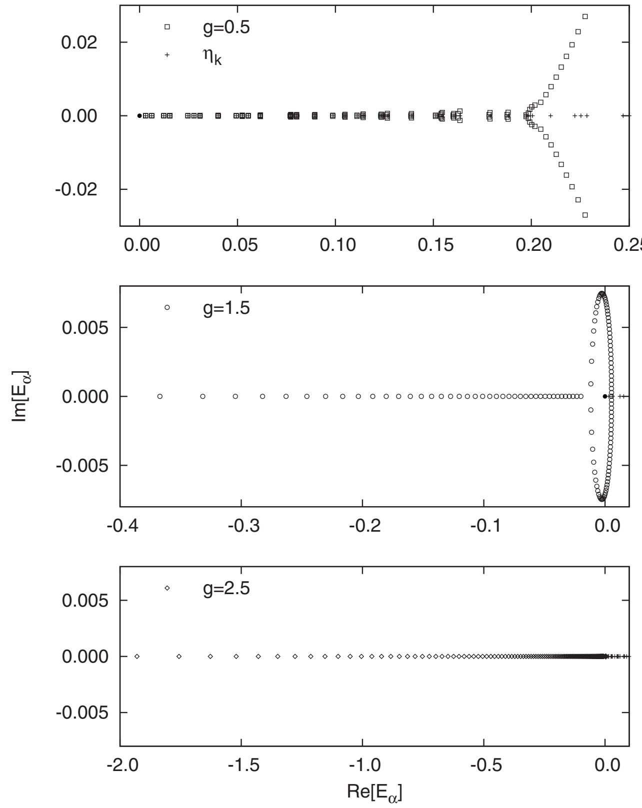

FIG. 3. Pairon distribution for $L=504$ at quarter filling, $\rho=0.25$, for $g=0.5$, $g=1.5$, and $g=2.5$.

Although easily written down, actually solving Eq. (17) for more than a few pairs turns out to be a cumbersome task due to singularities that occur when some of the pairons approach the origin or a certain level value η_k, or if two or more pairons approach each other. For the rational model with all $s_k=1/2$, where the singularities entail at most two pairons, Richardson already proposed a practical solution,[32] by rewriting Eq. (17) in terms of the real part of the pairon values and the square of the difference between two pairon values. If singularities with three or more pairons occur, this trick no longer works. More complicated change of variables have been proposed to remediate this problem for the rational model[30,31] but in the hyperbolic model we are confronted with a situation where *all* pairons can converge to zero and where the change of variables can no longer be performed with sufficient accuracy. Standard gradient methods to solve Eq. (17) directly run into problems because the Jacobian matrix becomes ill-conditioned well before the pairons reach the singularities.

Our numerical strategy to solve the RG equations is to start from an educated guess for the position of the M

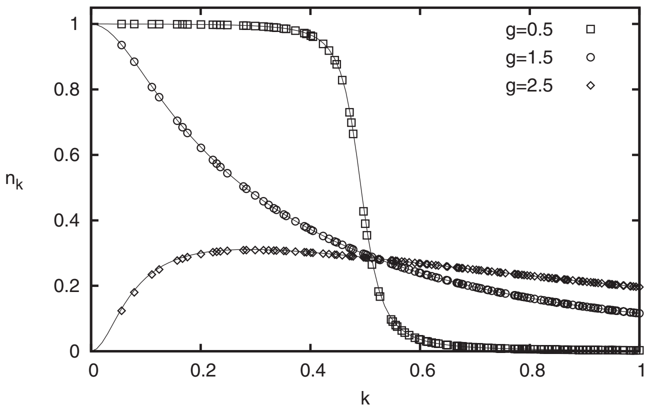

FIG. 4. Momentum density profiles, $n_k = \langle c_k^\dagger c_k \rangle$, for the same parameter sets as in Fig. 3 (see symbols), compared to the mean-field solution for the same system (continuous lines).

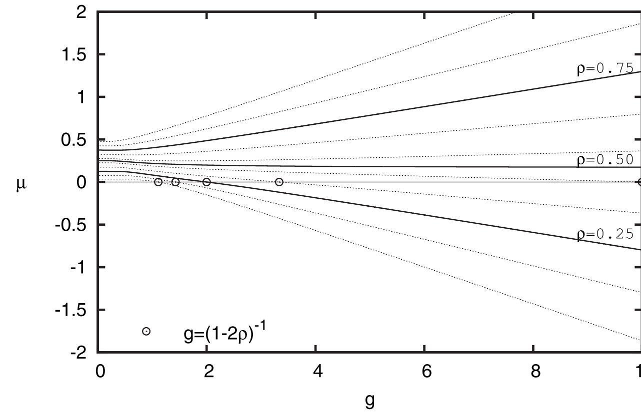

FIG. 6. Analytical results for the chemical potential μ as a function of g, for densities $\rho = 0.05, 0.15, \ldots, 0.95$, in ascending order. The symbols mark the transition points at $g = (1-2\rho)^{-1}$.

pairons in the weak-coupling limit. In this limit the RG equations decouple into M independent equations (one for each level). As discussed in Appendix B, the solution for each of these generalized Stieltjes equations is given by the roots of a Jacobi polynomial, which we use as a starting point for the iterative procedure at small values of G. The value of the coupling strength G is then gradually increased up to the desired value. At each step we solve Eq. (17) using a variation on the Levenberg-Marquardt algorithm,[33] where care has been taken to avoid singularities in the Jacobian matrix. In order to avoid the typical divergencies that burden the numerical procedures in intermediate steps, we modify the level parameters η_k and the central charge Q by adding a modulated artificial imaginary part. Once the desired value of G is obtained, a new iterative procedure is initiated, in which the imaginary parts of η_k and Q are gradually reduced to obtain the final solution. For the numerical results displayed in Figs. 2–11, we have taken the kinetic-energy cutoff $\omega = 1/2$, such that the level parameters η_k range from 0 to 1.

As a first illustration of the properties of the exact solution in the different regions of the quantum phase diagram, we treat ten pairs in a two-dimensional lattice in a disk geometry with a five unit cell radius. The system has a total active space of dimension $L = 2\Sigma_k s_k = 40$, hence this amounts to quarter filling, i.e., $\rho = 0.25$. The resulting level parameters are depicted in Table I and the spectral parameters E_α are shown in Fig. 2. In the extreme weak-coupling limit the ten pairs fill the lowest four levels. With increasing coupling the pairons expand in the complex plane lowering their real part, and consequently the total energy. There is a particular value of the scaled coupling strength $E_\alpha g = GL$ at which all pairons collapse to zero (the Moore-Read line), later on expelling one pairon with a negative real value. From this point up to the QPT at $Q = 0$ there are a series of collapses with nine, eight, etc., pairons, and after each one a new real negative pairon is produced. The exact solution for this small system shows the qualitative behavior of the pairons in the quantum phase diagram (Fig. 1). In order to get a more quantitative picture of the pairon distribution in the three regions of the quantum phase diagram, we plot in Fig. 3 the pairon distributions for three representative values of the coupling strength, $g = 0.5, 1.5, 2.5$, at quarter filling for a disk of radius 18 corresponding to a total pair degeneracy $L = 504$, indicated in Fig. 1 by their respective symbols.[34] One notes the distinctive features: in weak-coupling BCS part of the pairons

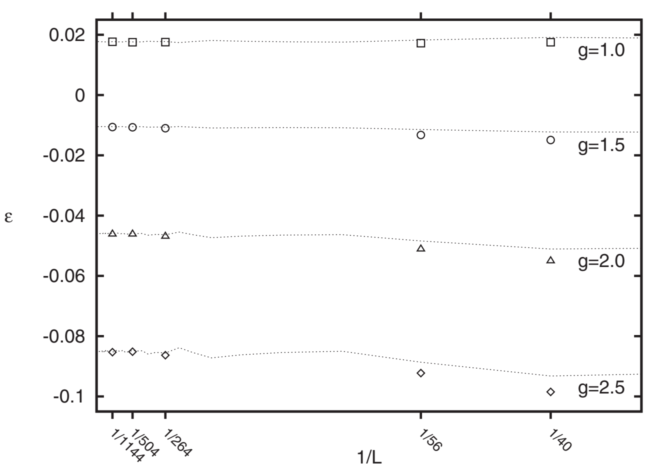

FIG. 5. Finite-size scaling of the energy density ε at quarter filling for several interaction strengths (corresponding to distinct regions of the phase diagram), both for the exact solution (symbols) as for the mean-field solution (lines).

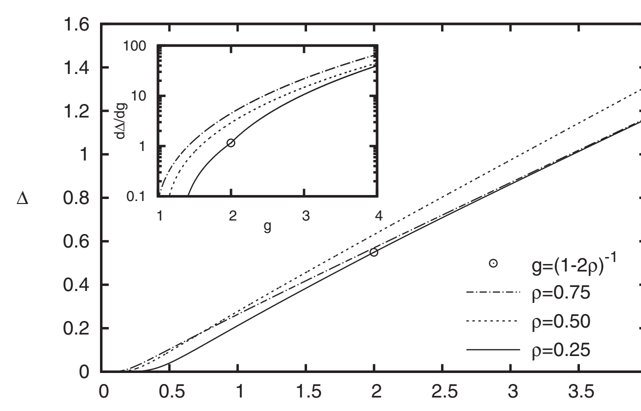

FIG. 7. Analytical results for the pairing field Δ and its derivative $d\Delta/dg$ in the inset, as a function of g for various densities.

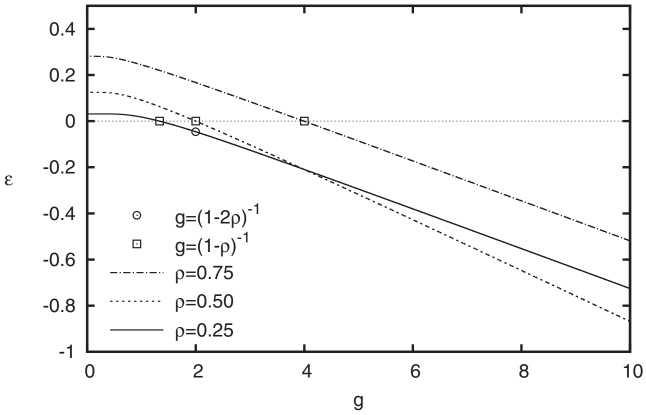

FIG. 8. Analytical results for the energy density ε of the integrable p_x+ip_y model as a function of the coupling strength g for representative densities ρ, in the thermodynamic limit. The symbol ⊙ marks the QPT point while ⊡ the Moore-Read line.

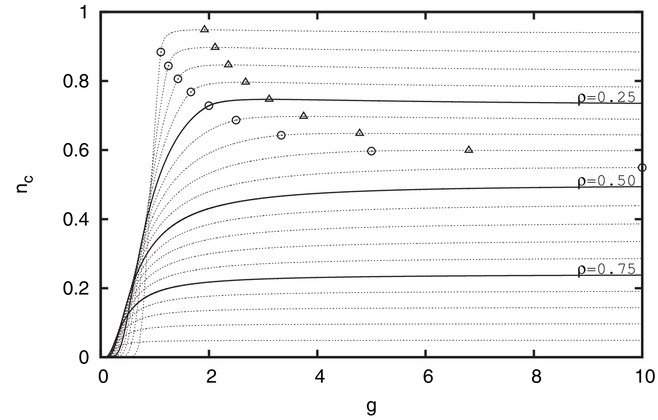

FIG. 10. Condensate fraction of pairs, n_c, as a function of g, for densities $\rho=0.05, 0.10, \ldots, 0.95$, in descending order. The circles mark the transition points at $g=(1-2\rho)^{-1}$ while the triangular symbols mark the point where n_c is maximal.

stick to the lower part of the real positive axis while the remaining pairons form a double arc in the complex plane. Approaching the Moore-Read line it looks like the arc is going to close around the origin, but just at the Moore-Read line all the pairons collapse to zero, and then a first real negative pairon emerges. In the intermediate weak-pairing region a successive series of collapses ensues, at integer values of Q, each time producing one more real negative pairon and reducing the size of the arcs around the origin. When the last pairon turns real and negative, the system enters the strong-pairing phase. From then on the most negative pairon diverges proportional to the interaction strength G, while the least negative pairon converges to a finite value that can be related to the condensate fraction, as we will see later on.

In Fig. 4 we show the momentum density distributions corresponding to each of the configurations in Fig. 3. In the weak-pairing region one sees that the lowest momentum states are fully occupied. On the other side of the phase transition the lowest momentum states are vacated, resulting in a nontrivial topology for the two-dimensional momentum distribution.

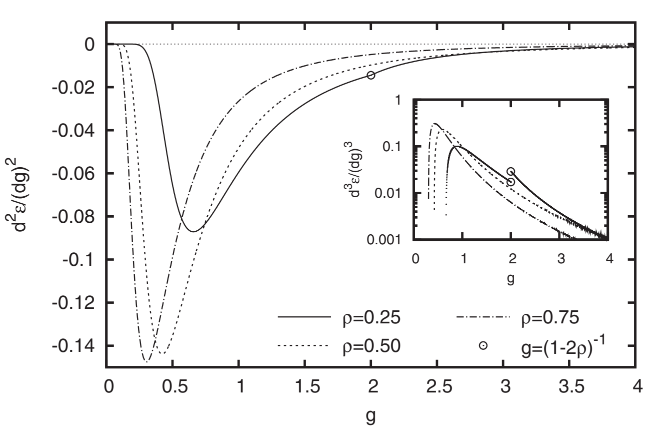

FIG. 9. Higher order derivatives of the energy density ε as a function of g for various densities. The small circles mark the transition point at $g=(1-2\rho)^{-1}$.

B. Thermodynamic limit

We are interested in determining the quantum phase diagram of the integrable p_x+ip_y model defined by Hamiltonian (22). To explore the possible QPTs we have to properly define the thermodynamic limit for this model. From Fig. 5 we see that for large systems the exact solution and the mean-field solution tend to the same results. Particularly, in mean-field theory one observes that for static values of the chemical potential μ and the pairing field Δ, the quantities M, E, and G^{-1} scale proportional with L. We can describe the thermodynamic limit when L goes to infinity in terms of intensive quantities such as the scaled interaction strength $g=GL$ and the density $\rho=M/L$. At the same time we have to establish a cutoff ω in kinetic energy, such that the energy density $\varepsilon=E/L$ remains finite, and a density of levels $\varrho(\eta)$, such that $\int_0^{2\omega}\varrho(\eta)d\eta=1$. The cutoff ω determines the energy scale of the problem. It can be renormalized by relating it to the energy of a single pair as explained in Appendix A.

As demonstrated in Appendices C and D, for intensive quantities, the exact solution and the mean-field solution co-

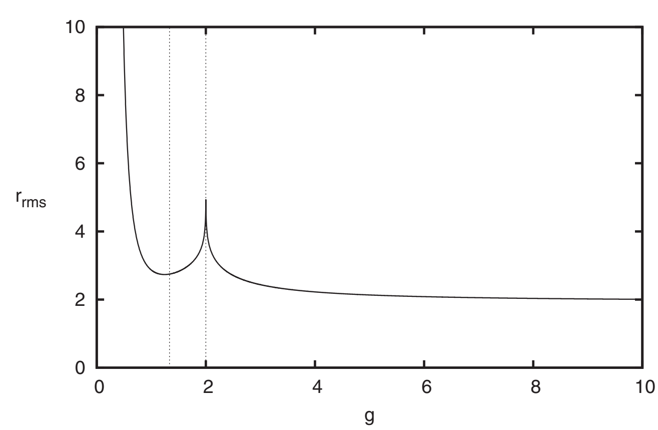

FIG. 11. Root-mean-square radius, r_{rms}, of the condensate wave function in units of $1/\sqrt{2\omega}$, at quarter filling. The dashed lines indicate the Moore-Read point ($\varepsilon=0$) and the phase-transition point ($\mu=0$).

TABLE I. Level parameters η_k and s_k for a disk with a radius of five unit cells in a two-dimensional square lattice.

η_k	0.04	0.08	0.16	0.20	0.32	0.36	0.40	0.52	0.64	0.68	0.72	0.80	1.00
s_k	1	1	1	2	1	1	2	2	1	2	1	2	3

incide in the thermodynamic limit and yield the following integral equations:

$$\int_0^{2\omega} \varrho(\eta)\frac{\eta}{\sqrt{(\eta-2\mu)^2+4\eta\Delta^2}}d\eta=\frac{1}{g}, \tag{29}$$

$$\int_0^{2\omega} \varrho(\eta)\frac{2\mu}{\sqrt{(\eta-2\mu)^2+4\eta\Delta^2}}d\eta=\frac{1}{g}-1+2\rho. \tag{30}$$

Note that the chemical potential μ and the pairing field Δ^2 scale proportional to ω, and can be determined from the self-consistent solution of the above equations (see Figs 6 and 7). The energy density in the thermodynamic limit is given by

$$\varepsilon=\frac{\omega}{2}+\mu(2\rho-1)+\frac{\Delta^2}{g}-\frac{1}{2}\int_0^{2\omega}\varrho(\eta)\sqrt{(\eta-2\mu)^2+4\eta\Delta^2}d\eta. \tag{31}$$

One sees that Eqs. (29) and (30) coincide with the conditions

$$\frac{\partial\varepsilon}{\partial\mu}=0, \quad \frac{\partial\varepsilon}{\partial\Delta}=0, \tag{32}$$

meaning that the mean-field solution minimizes the energy written as a function of the mean-field parameters μ and Δ.

For the two-dimensional p_x+ip_y model one finds that $\varrho(\eta)=1/(2\omega)$, and one can solve the integral appearing in Eq. (31) analytically

$$\begin{aligned}\varepsilon=&\frac{\omega}{2}+\mu(2\rho-1)+\frac{\Delta^2}{g}+\frac{|\mu|(\Delta^2-\mu)}{2\omega}\\&-\frac{\omega+\Delta^2-\mu}{2\omega}\sqrt{(\omega-\mu)^2+2\omega\Delta^2}\\&+\frac{\Delta^2(\Delta^2-2\mu)}{2\omega}\ln\left(\frac{\omega+\Delta^2-\mu+\sqrt{(\omega-\mu)^2+2\omega\Delta^2}}{\Delta^2-\mu+|\mu|}\right).\end{aligned} \tag{33}$$

From Eq. (32) we obtain explicit expressions for g and ρ,

$$\begin{aligned}g^{-1}=&\frac{1}{\omega}\Bigg[\sqrt{(\omega-\mu)^2+2\omega\Delta^2}-|\mu|\\&+(\mu-\Delta^2)\ln\left(\frac{\omega-\mu+\Delta^2+\sqrt{(\omega-\mu)^2+2\omega\Delta^2}}{\Delta^2-\mu+|\mu|}\right)\Bigg],\end{aligned} \tag{34}$$

$$\begin{aligned}\rho=&\frac{1}{2}-\frac{1}{2\omega}\Bigg[\sqrt{(\omega-\mu)^2+2\omega\Delta^2}-|\mu|\\&-\Delta^2\ln\left(\frac{\omega-\mu+\Delta^2+\sqrt{(\omega-\mu)^2+2\omega\Delta^2}}{\Delta^2-\mu+|\mu|}\right)\Bigg].\end{aligned} \tag{35}$$

This allows us to rewrite Eq. (33) in a more elegant form

$$\varepsilon=\rho(\omega+\mu)+\frac{\Delta^2}{2g}-q\frac{\omega\Delta^2}{\mu}-\frac{\mu+|\mu|}{2}, \tag{36}$$

where

$$q=Q/L=\frac{1}{2g}-\frac{1}{2}+\rho. \tag{37}$$

The appearance of the absolute value of μ clearly indicates that there exists a nonanalyticity in ε at $\mu=0$.

Before closing this section we would like to point out that even though the RG equation in the thermodynamic limit coincides with the mean-field gap equation, strictly speaking, the mean-field and exact solutions are not the same. It is obvious that the mean-field state does not preserve the total number of particles $2M$ while the exact solution does. In the thermodynamic limit however the total energy per particle ($e=E/2M=E_{\text{mf}}/2M$) becomes the same. Obviously, if two variational states reproduce the exact ground-state energy in the thermodynamic limit and if the ground state is not degenerate then the two variational states have to be the same in this limit but this is not the case here. This is not a paradox because the density fluctuations are gapless and the two functions (E and E_{mf}) differ by square-root fluctuations of M. The same happens for other observables.

C. Derivatives of the energy density

The third term of Eq. (36) might suggest a singularity in ε at $\mu=0$ and hence a zeroth-order QPT at this point. However, it turns out that $\mu=0$ coincides with $q=0$ such that the singularity in ε is canceled out and as a result ε is a continuous function of g and ρ over the whole parameter range. A special point that one observes in Eqs. (34) and (35) corresponds to $\mu=\Delta^2/2$, which leads to $g^{-1}=1-\rho$. This is the *Moore-Read* line we discussed in Sec. II B. As argued above and as can be seen from Fig. 8, the energy vanishes at this point but is continuous. Consequently, there is no zeroth-order QPT in this model (contrary to previous reports in the literature[18,22]).

The fourth term in Eq. (36) might suggest a discontinuity in the derivative $d\varepsilon/d\mu$ at $\mu=0$. However, it turns out that the third term also has a discontinuity in its derivative that exactly cancels the one in the fourth term. To formalize this, let us consider the derivatives of ε with respect to ρ and g,

$$\frac{\partial \varepsilon}{\partial \rho} = 2\mu, \quad \frac{\partial \varepsilon}{\partial g} = -\Delta^2/g^2. \tag{38}$$

In Eqs. (34) and (35) we see that g^{-1} and ρ are continuous functions of μ and Δ. Hence, μ and Δ are continuous functions of ρ and g, and therefore the derivatives of ε with respect to ρ and g are continuous functions of ρ and g. We conclude that there is no first-order QPT in this model. Note also that in the strong-coupling limit Δ tends to the same value for ρ=0.25 and ρ=0.75 (see Fig. 7). This is a consequence of the symmetry that we will discuss in Sec. IV.

For higher order derivatives, we resort to a graphical representation (an outline for their analytic derivation is given in Appendix E). From Fig. 9 we see that there is a discontinuity in the third-order derivative of ε. The discontinuity occurs when μ=0. If we set μ=0 in Eqs. (34) and (35), we find that this coincides with $g^{-1}=1-2\rho$. This transition line has been identified in previous works as the Read-Green line.[14,18] We see that a third-order QPT occurs at this line, for densities below half filling, i.e., $\rho \leq 1/2$.

D. Characterization of the superfluid phases

In s-wave pairing models (rational RG model) the transition from a weak- to a strong-pairing phase is often described in terms of a "BCS-BEC" crossover, where on the weak side one has dilute pairs moving in a coordinated way as described by BCS theory while on the strong side the fermion pairs behave as molecules that become perfect bosons in the strong-coupling limit, where they form a pure BEC. In the p_x+ip_y case the picture differs in an essential way: we see that instead of a crossover there is a sharp third-order QPT at $g^{-1}=1-2\rho$.

Because the exact few points ground-state correlation functions coincide with the mean-field ones in the thermodynamic limit, we can use Eq. (D17) to evaluate the condensate fraction n_c, following the standard definition of Yang:[35]

$$\begin{aligned} n_c &= \frac{1}{M}\sum_{k,k_x>0} |\langle S_k^- \rangle|^2 \\ &= \frac{L\Delta^2}{2\omega M}\int_0^{2\omega} \frac{\eta}{(\eta-2\mu)^2+4\eta\Delta^2} d\eta \\ &= \frac{\Delta^2}{2\omega\rho}\,\frac{a\,\ln(1-2\omega/a)-b\,\ln(1-2\omega/b)}{a-b}, \end{aligned} \tag{39}$$

where a and b are such that

$$(\eta-2\mu)^2+4\eta\Delta^2 = (\eta-a)(\eta-b).$$

As explained in Appendix C, a and b are the lower and upper bounds of the line of pairons in strong pairing in the thermodynamic limit. We have used the mean-field expectation values because they coincide with the exact results in the thermodynamic limit. For finite systems one could evaluate the exact correlation functions using techniques similar to the ones presented in Ref. 36 for the rational RG model. Figure 10 displays the results for various densities. One observes that a pair condensate develops at large interaction strength. Two features draw attention: first of all, we see that for a fixed density $\rho < 1/2$ the condensate fraction reaches a maximum in the strong-pairing phase at a finite value of g, and then slightly decreases to its limiting value for $g \to \infty$. This means that the fermion pairs do not behave as pure bosons, but rather as bound molecules with a certain spatial extension, such that the Pauli principle prohibits a complete condensation of all molecules.[37] Secondly, note that because we study here the condensate fraction as a function of the interaction strength, the limiting value of n_c in the strong BEC limit is not 1, contrary to what one is accustomed to in three dimensions for the s-wave case,[38] where one evaluates n_c as a function of the ratio between interparticle distance and scattering length.

To understand the behavior of the condensate fraction in the strong-coupling limit, we evaluate μ and Δ^2 for $g \gg 1$ up to leading order in g,

$$\mu \sim -2\omega g(1-2\rho/3)(1-2\rho)/4, \tag{40}$$

$$\Delta^2 \sim 2\omega g^2(1-2\rho/3)^2\rho/2. \tag{41}$$

Using the expressions for a and b in terms of μ and Δ^2 from Appendix C, and substituting these in Eq. (39), one finds that in the strong-coupling limit

$$\lim_{L\to\infty, g\to\infty} n_c = \frac{1}{4\rho}\left[1-\frac{(1-2\rho)^2}{4\rho}\ln\left(\frac{1+2\rho}{1-2\rho}\right)\right]. \tag{42}$$

At low densities, this expression approaches Yang's bound for the condensate fraction of a generic fermionic superfluid,[35] $n_c \leq 1-\rho$.

Given that there is a condensate, it is worthwhile to analyze the corresponding condensate wave function in momentum space, which in the thermodynamic limit is given by[35]

$$\phi_{\text{Yang}}(k) = u_k v_k \propto \frac{k_x - ik_y}{\sqrt{(k^2-a)(k^2-b)}}. \tag{43}$$

The condensate wave function has an inherent length scale r_{rms} that can be calculated as[38]

$$r_{\text{rms}}^2 = \int |\nabla\phi(k)|^2 dk \Big/ \int |\phi(k)|^2 dk. \tag{44}$$

After some algebra, one obtains the analytical expression

$$r^2_{\text{rms,Yang}} = \frac{2\omega[ab-(a+b)\omega]\left[\dfrac{1}{(2\omega-a)^2}+\dfrac{1}{(2\omega-b)^2}\right]+\dfrac{a^2-4ab+b^2}{a-b}[\ln(1-2\omega/a)-\ln(1-2\omega/b)]}{(a-b)[a\ln(1-2\omega/a)-b\ln(1-2\omega/b)]}. \tag{45}$$

The resulting radius $r_{\text{rms,Yang}}$ is plotted in Fig. 11. One sees that it goes to a finite value in the strong-coupling limit, and that it diverges at the QPT, with a singularity in the function $\ln(1-2\omega/a)$, that scales as $\ln|\mu|$. The condensate wave function can be related directly to observable quantities: from Wick's theorem for the mean-field solution one obtains

$$\langle c_r^\dagger c_{r'}^\dagger\rangle\langle c_{r'}c_r\rangle = \langle c_r^\dagger c_{r'}^\dagger c_{r'}c_r\rangle - \langle c_r^\dagger c_r\rangle\langle c_{r'}^\dagger c_{r'}\rangle + \langle c_r^\dagger c_{r'}\rangle\langle c_{r'}^\dagger c_r\rangle. \tag{46}$$

We can rewrite this as

$$|\phi_{\text{Yang}}(r-r')|^2 \propto \langle(n_r-\langle n_r\rangle)(n_{r'}-\langle n_{r'}\rangle)\rangle + |F(r-r')|^2, \tag{47}$$

where $\phi_{\text{Yang}}(r)$ is the condensate wave function in coordinate space and $F(r)$ is the Fourier transform of the momentum density $\langle c_k^\dagger c_k\rangle$. In trapped Fermi gases the first term on the right-hand side of Eq. (47) can be obtained through quantum noise interferometry[39] while the momentum density and hence $F(r)$ can be obtained from a time-of-flight analysis after releasing the trap. Once these quantities are known, one can calculate the radius $r_{\text{rms,Yang}}$. Therefore this length scale is an experimentally accessible quantity that would give a clear signature of the third-order QPT in the p_x+ip_y superfluid.

We can apply a similar analysis to the Bethe ansatz solution: in Eq. (8) we see that the exact eigenstates are given by a product of pair wave functions,

$$\mathrm{S}^+(E_\alpha) = \sum_k \phi_{E_\alpha}(k)c_k^\dagger c_{-k}^\dagger \quad \text{with} \quad \phi_E(k) \propto \frac{k_x+ik_y}{k^2-E}. \tag{48}$$

The ground state is given by a set of pairon values E_α and hence can be interpreted as an ensemble of Cooper pairs of varying size.[38,40] Evaluating the root-mean-square radius for the Cooper pair wave function $\phi_E(r)$ in coordinate space, one finds that

$$r^2_{\text{rms},E} = 8\frac{2\omega\,\mathrm{Re}[E](\mathrm{Re}[E]-2\omega)\left(\dfrac{1}{2\omega-E}-\dfrac{1}{2\omega-E^*}\right)+|E|^2[\ln(1-2\omega/E^*)-\ln(1-2\omega/E)]}{(E-E^*)^2[E\ln(1-2\omega/E)-E^*\ln(1-2\omega/E^*)]}, \tag{49}$$

$$= \frac{4\omega(3E^2-6\omega E+8\omega^2)}{3E(E-2\omega)^3[\ln(1-2\omega/E)+2\omega/(E-2\omega)]}, \quad \text{for } E \text{ real and negative}. \tag{50}$$

This length scale is finite if E is complex, and converges to a finite value when E approaches the real negative axis. But when approaching real and positive values of E, inside the interval $[0,2\omega]$, the length scale $r_{\text{rms},E}$ diverges. The exact solution of the integrable p_x+ip_y model gives us a beautiful insight into the nature of the QPT: in strong pairing all pairon values E_α are real and negative, which means that the exact ground state corresponds to an ensemble of confined Cooper pairs (bound molecules) with finite radius. Lowering the interaction strength one encounters the QPT at which one pairon value becomes real and positive, which corresponds to a single deconfined Cooper pair on top of the ensemble of confined Cooper pairs. Further in the weak-pairing phase, more and more pairons become complex, realizing a mixture of bound molecules (negative pairons) and Cooper resonances (complex pairons). At integer values of $2Q$ there are $2Q+1$ complex pairons that collapse to zero giving rise to deconfined Cooper pairs while at intermediate values part of the pairons form a closed curve around the origin in the complex plane, some stick to the lowest part of the real positive axis (inside the closed curve) and the remaining ones stay confined on the real negative axis outside the closed curve. At the Moore-Read line all Cooper pairs are deconfined. From there on the pairon curve opens up in two arcs and part of the Cooper pairs form resonances of finite size (complex pairon values), till all Cooper pairs convert to plane waves in the extreme weakly interacting limit. Hence we can understand the QPT as a confinement-deconfinement phase transition.

IV. SYMMETRIES OF THE RICHARDSON-GAUDIN EQUATIONS

In this section we highlight some symmetry relations of the RG equations that allow us to relate states in the strong-pairing phase with mirror states in the weak-pairing range that have the same energy.[18] To set the stage we would like to introduce a new set of operators,

$$\{T_m^+, T_m^-, T_m^z\} \quad \text{with } m = \dots, -2, -1, 0, 1, 2, \dots, \tag{51}$$

which form an affine Lie algebra

$$[T_m^+, T_{m'}^-] = 2T_{m+m'}^z, \quad [T_m^z, T_{m'}^{\pm}] = \pm T_{m+m'}^{\pm}. \tag{52}$$

A possible representation of these elements of the algebra in terms of $su(2)$ spin operators is ($\sigma = z, \pm$),

$$T_m^\sigma = \sum_i (\eta_i)^{m/2} S_i^\sigma, \tag{53}$$

for (in principle arbitrary) quantum number i.

It is straightforward to check that the following two families of Hamiltonians:

$$H_r = T_{2m}^z - GT_0^+ T_0^-, \tag{54}$$

$$H_h = T_{2m}^z - GT_m^+ T_m^-, \tag{55}$$

define the integrable rational and hyperbolic RG models of Eq. (16). It is illuminating to solve those integrable rational and hyperbolic models in terms of the generators of the affine Lie algebra. The eigenvectors can generically be written as in Eq. (8) with (unnormalized)

$$\mathsf{S}^{\pm}(E_\alpha) = \sum_{m=0}^{\infty} \frac{G}{E_\alpha^{m+1}} T_{2m}^{\pm}, \quad E_\alpha \neq 0,$$

$$\mathsf{S}^{\pm}(0) = T_{-2}^{\pm}, \quad \text{rational model}, \tag{56}$$

$$\mathsf{S}^{\pm}(E_\alpha) = \sum_{m=0}^{\infty} \frac{2\gamma\sqrt{E_\alpha}}{E_\alpha^{m+1}} T_{2m+1}^{\pm}, \quad E_\alpha \neq 0,$$

$$\mathsf{S}^{\pm}(0) = T_{-1}^{\pm}, \quad \text{hyperbolic model}, \tag{57}$$

where E_α are the pairons. Notice that to represent these eigenvectors one needs an infinite set of generators, the even series for the rational model and the odd for the hyperbolic model. In terms of the affine operators one can demonstrate some interesting symmetry properties of the model:

Theorem 1. Given the hyperbolic Hamiltonian H_h, and a particular eigenstate $|\Phi_M\rangle$ of order $M \leq (L - G^{-1})/2$, for integer values of $G^{-1} = L - 2M + 1 - N$, there exists another eigenstate $|\Phi_{M+N}\rangle = (T_{-1}^+)^N |\Phi_M\rangle$ with the same energy E.

Proof. Define $H_h = T_2^z - GT_1^+ T_1^-$. One can straightforwardly evaluate the commutators

$$[H_h, T_{-1}^+] = T_1^+ + 2GT_1^+ T_0^z, \tag{58}$$

$$[[H_h, T_{-1}^+], T_{-1}^+] = 2GT_1^+ T_{-1}^+. \tag{59}$$

Now let us consider a state of the form

$$|\Phi_{M+N}\rangle = (T_{-1}^+)^N |\Phi_M\rangle. \tag{60}$$

We want to determine the conditions for $|\Phi_{M+N}\rangle$ to be an eigenstate if $|\Phi_M\rangle$ is another eigenstate of H_h of energy E. Using the commutation relations above we have

$$[H_h, (T_{-1}^+)^N] = N(T_{-1}^+)^{N-1} T_1^+ [1 + 2GT_0^z + G(N-1)]. \tag{61}$$

Therefore

$$H_h |\Phi_{M+N}\rangle = E|\Phi_{M+N}\rangle + N(T_{-1}^+)^{N-1} T_1^+ [1 + G(2M - L + N - 1)] \times |\Phi_M\rangle. \tag{62}$$

The condition to be an eigenstate is

$$G^{-1} = L - N - 2M + 1. \tag{63}$$

This means that for a certain value of $G = 1/(L - M - M' + 1)$, there exist two states, one of order M and another state of order M', that have the same energy E. From this algebraic relation, one can distinguish the two special cases already mentioned in Sec. II B.

Special case (i). A first case is the symmetric case that occurs when $M = M'$, i.e., when

$$M = (L + 1 - G^{-1})/2, \quad Q = -\frac{1}{2}. \tag{64}$$

Special case (ii). Another special case occurs when $M' = 0$, which amounts to

$$M = L + 1 - G^{-1}, \quad Q = \frac{M-1}{2}. \tag{65}$$

The corresponding eigenstate of order M is given by $|0_M\rangle = (T_{-1}^+)^M |\nu\rangle$. The energy of this state is equal to the vacuum energy, $E(0_M) = \langle \nu | H_h | \nu \rangle$. Comparing this state with the Bethe ansatz from Eq. (8), one observes that this state corresponds to the case where the M pairons converge to 0.

These algebraic relations are easily recognized to be symmetries of the RG equations as well. Consider Eqs. (17) and (18) for $G^{-1} = L - 2M + 1 - N$, and evaluate Eqs. (17) and (18) for the cases with M and $M+N$ pairs, where N pairons E_β, $\beta = M+1, \dots, M+N$, are zero. Then, Q for the M pair case is given by $Q = -(N+1)/2$ while for the $M+N$ situation it is $Q = -(N+1)/2 + N$. On the other hand, the first term in Eq. (17) is the same for M or $M+N$ but the second one differs precisely by N/E_α so that it cancels with the $-N/E_\alpha$ coming from the third term. The bottom line is that the RG equations remain the same for the two cases M and $M+N$.

In the thermodynamic limit this symmetry manifests itself as a particular transformation of the chemical potential μ and gap Δ which preserves the form of Eqs. (29) and (30). For certain values of μ and Δ^2 there exists another set of values μ' and Δ'^2 that lead to the same equations,

$$\mu' = -\mu, \tag{66}$$

$$\Delta'^2 = \Delta^2 - 2\mu. \tag{67}$$

The theorem above relates eigenstates belonging to different Hilbert subspaces for particular values of G and is a result also obtained in Ref. 22 in the context of the $p_x + ip_y$ superfluid. By using the affine Lie algebra introduced in Eq. (52), we have generalized this result to arbitrary realizations and representations of the general hyperbolic RG model. One may wonder whether a similar symmetry property holds for the rational RG model $H_r = T_2^z - GT_0^+ T_0^-$. Let us assume that there exists a state

$$|\Phi_{M+N}\rangle = (T_{-2}^+)^N |\Phi_M\rangle \tag{68}$$

and determine the conditions to be an eigenstate of H_r whenever $|\Phi_M\rangle$ is. The commutator

$$[H_r,(T_{-2}^+)^N] = N(T_{-2}^+)^{N-1}[H_r,T_{-2}^+] + \frac{N(N-1)}{2}(T_{-2}^+)^{N-2}[[H_r,T_{-2}^+],T_{-2}^+] \tag{69}$$

implies that the action of the Hamiltonian on the state [Eq. (68)] is

$$H_r|\Phi_{M+N}\rangle = E|\Phi_{M+N}\rangle + N(T_{-2}^+)^{N-2}T_0^+[T_{-2}^+(1+2GT_{-2}^z) + G(N-1)T_{-4}^+]|\Phi_M\rangle. \tag{70}$$

To cancel out the second term two conditions need to be satisfied. First, the number of pairons with $E_\alpha=0$ must be $N=1$. Second,

$$(1+2GT_{-2}^z)|\Phi_M\rangle = 0, \tag{71}$$

which indicates that for a particular value of G, satisfying the relation above, a state with at most *one* zero pairon may exist in the rational model, as opposed to the hyperbolic case where states with an arbitrary number of zero pairons are possible eigenvectors. This qualitative difference reflects in the quantum phase diagram. While the hyperbolic model displays a QPT from a weak-pairing phase to a strong-pairing phase, the rational model displays a crossover. This is so, since the symmetry relation indicates that at the $\mu=0$ line the ground state becomes degenerate, while this is not the case in the rational model. Connecting points with equal energies in the phase diagram, we see that they form two lines (one in weak pairing and one in strong pairing) that approach the phase-transition line at the same point but under different angles. Hence it is no surprise that the energy is continuous but has a discontinuity in the third-order and higher order derivatives at this point.

Another interesting symmetry relation, not discussed before, emerges by considering the integrable Hamiltonian

$$\tilde{H}_h = T_{-2}^z - \tilde{G}T_{-1}^+ T_{-1}^-, \tag{72}$$

which is another exactly solvable hyperbolic RG Hamiltonian, corresponding to parameters $\tilde{\eta}_i = 1/\eta_i$. A simple way to derive it is to make the choice $\epsilon_i = \tilde{\lambda}\eta_i^{-1}$ in Eq. (2).

Theorem 2. Given the hyperbolic Hamiltonian H_h, there exists another $\tilde{H}_h$ with $\tilde{G}^{-1} = L - 2M + 2 - G^{-1}$ whose eigenstates are the same but the eigenvalues are given by $\tilde{E} = \langle\nu|\tilde{H}_h|\nu\rangle + \Sigma_\alpha E_\alpha^{-1}$. Hence, although $\tilde{H}_h$ must have the same eigenstates as H_h for the same Hilbert subspace of order M, their eigenvalues are different.

Proof. We explore now how the eigenvalues of $\tilde{H}_h$ are related to those of H_h. The commutator with H_h is given by

$$[H_h,\tilde{H}_h] = (T_1^+ T_{-1}^- - T_{-1}^+ T_1^-)[2G\tilde{G}(1-T_0^z) - G - \tilde{G}]. \tag{73}$$

Acting on a state of order M it results

$$[H_h,\tilde{H}_h]|\Phi_M\rangle = [G\tilde{G}(L-2M+2) - G - \tilde{G}](T_1^+ T_{-1}^- - T_{-1}^+ T_1^-) \times |\Phi_M\rangle. \tag{74}$$

Therefore, for given values of G and M the relation

$$\tilde{G}^{-1} + G^{-1} = L - 2M + 2 \tag{75}$$

defines a value of $\tilde{G}$ such that $[H_h,\tilde{H}_h]=0$. This algebraic identity also shows up in Eq. (17) since these equations are invariant under the transformation

$$\tilde{\eta}_i = \eta_i^{-1}, \quad \tilde{E}_\alpha = E_\alpha^{-1}, \quad \tilde{G}^{-1} = L - 2M + 2 - G^{-1}. \tag{76}$$

Hence one can conclude that for a given eigenstate $|\Phi_M\rangle$ of H_h, the following relation holds:

$$\langle\Phi_M|\tilde{H}_h|\Phi_M\rangle = \langle\nu|\tilde{H}_h|\nu\rangle + \sum_\alpha E_\alpha^{-1}. \tag{77}$$

In particular, at $G^{-1} = L - 2M + 2$, the state $|\Phi_M\rangle$ becomes an eigenstate of the operator $T_{-1}^+ T_{-1}^-$.

V. CONCLUSIONS

The exactly solvable hyperbolic RG model allows a parametrization that leads to a pairing model for spinless fermions in two dimensions with a p-wave interaction of $p_x + ip_y$ character. The model can be solved with a Bethe ansatz, even for large system sizes, using a numerical technique introduced in this paper. The thermodynamic limit can be evaluated analytically, leading to expressions for the ground-state energy density and few-body correlation functions that coincide with mean-field theory.

Even though the $p_x + ip_y$ model has been studied before,[18,22] we reach drastically different conclusions about the zero-temperature quantum phase diagram. Our numerical and analytical results show that the quantum phase diagram exhibits a third-order quantum phase transition when the chemical-potential changes sign. Most importantly, as shown in this paper, this transition is characterized by a logarithmically diverging length scale that can be obtained experimentally from correlations in the density fluctuations. This length scale can be associated with the size of the Cooper pairs making up the correlated many-body state. Those Cooper pairs, tightly bound in the strong-pairing phase, start to deconfine at the QPT point where $\mu=0$. Thus, in a certain sense, our physical picture is that the strong-pairing region represents a confined superfluid phase while the weak-pairing region is the deconfined phase. Similarly to many other examples of phase transitions which are not of the Landau type, as for instance in lattice gauge theories, the transition is not associated with any broken symmetry and thus has no local order parameter.

We show that these are general features of the hyperbolic RG model, irrespective of the specific symmetry or dimensionality of the representation. This means that our conclusions equally apply to other models derived from the same generalized Gaudin algebra, be it models for pairing in atomic nuclei, or Jaynes-Cummings-type models of resonantly coupled fermionic atoms. Furthermore, the algebraic underpinnings of the hyperbolic RG model allow us to demonstrate that there exists a transformation that relates states in strong pairing with states in weak pairing, and that the phase-transition line corresponds to the states that are symmetric under this transformation.

Finally, we would like to emphasize the fact that the phase diagram is based on the exact solution, which guarantees that the phase transition is not an artifact of the mean-field approximation. Moreover, Hamiltonian (1) is integrable for attractive and repulsive interactions while there is no mean-field solution in the yet unexplored repulsive case. Therefore, exact solvability could be a unique tool to investigate repulsive p-wave interactions.

ACKNOWLEDGMENTS

We thank M. Ibañez, G. Sierra, and R. Molina for interesting discussions. This work was supported by the Lundbeck Foundation, and the Marie Curie Actions of the European Community (Project No. 220335) and by the Spanish Ministry for Science and Innovation (FIS2009-07277).

APPENDIX A: ONE PAIR

Already the state with one pair leads to a non-trivial result. Equation (17) reduces to

$$\frac{Q}{E_1} + \frac{1}{2}\sum_{k,k_x>0} \frac{1}{E_1 - \eta_k} = 0. \tag{A1}$$

In order to solve this equation, we have to specify the space in which the model is defined. Let us consider a disk in momentum space, with radius aR such that R is integer and a is the spacing between successive momentum states. The kinetic-energy dispersion is given by $k^2/2$, which means that there is a kinetic-energy cutoff $\omega=(aR)^2/2$. In the continuum limit, corresponding to $R \gg 1$, one can take $L=\pi R^2/2$ and replace the sums over k by integrals with $dk_x=dk_y=a$,

$$\begin{aligned}\sum_{k,k_x>0} f(k^2) &\cong \frac{1}{a^2}\int\int_{k_x>0,k<aR} f(k^2)dk_x dk_y \\ &= \frac{\pi}{a^2}\int_{k=0}^{aR} f(k^2)kdk \\ &= \frac{\pi R^2/2}{(aR)^2}\int_0^{(aR)^2} f(\eta)d\eta \\ &= \frac{L}{2\omega}\int_0^{2\omega} f(\eta)d\eta. \end{aligned}\tag{A2}$$

Hence,

$$\begin{aligned}\sum_{k,k_x>0}\frac{1}{E_1-k^2} &= \frac{L}{2\omega}\int_0^{2\omega}\frac{1}{E_1-\eta}d\eta \\ &= -\frac{L}{2\omega}\ln\left(1-\frac{2\omega}{E_1}\right).\end{aligned}\tag{A3}$$

Substituting this result in Eq. (A1), one obtains that

$$2(Q/L)\frac{2\omega}{E_1} - \ln\left(1-\frac{2\omega}{E_1}\right) = 0. \tag{A4}$$

In the limit $L \gg 1$ one finds that $E_1=2\omega/f_g$, where $g=GL$ and f_g is the solution of the following equation:

$$(1/g - 1)f_g = \ln(1-f_g). \tag{A5}$$

If $1/g<1$, then $f_g<0$ and one obtains a ground-state energy for one pair,

$$E_1 = 2\omega/f_g, \tag{A6}$$

such that $E_1<0$. This value E_1 then defines a physical energy scale that can be used to eliminate the cutoff ω as done in Ref. 16. For $1/g \geq 1$, the one-pair ground state corresponds to a nonpaired state with $E_1=0$. In this case there is no relevant energy scale to renormalize the cutoff.

The one-pair energy is a physically meaningful quantity that allows one to relate different models describing the same physics. Typically, models with p_x+ip_y pairing will have an interaction that scales as $(k_x+ik_y)(k'_x-ik'_y)$ for small k, just like the integrable p_x+ip_y model but for large momenta the interaction could be very different. Because the peculiarities of the quantum phase diagram are determined mainly by the small-k behavior, we expect similar results for other two-dimensional p_x+ip_y models, as, e.g., in Ref. 16. To relate their results to ours, one has to renormalize the interaction strength, which can be done by equating the one pair energy.

APPENDIX B: POLYNOMIAL SOLUTION FOR THE ONE-LEVEL MODEL

In the limiting case of a single level, $l=1$, Eq. (17) takes the form

$$\frac{s}{\eta - E_\alpha} - \sum_{\alpha',\alpha'\neq\alpha}\frac{1}{E_{\alpha'}-E_\alpha} = \frac{Q}{E_\alpha}, \quad \forall \quad \alpha. \tag{B1}$$

Equation (B1) is a generalized Stieltjes equation[41] that can be solved by multiplying it by $2E_\alpha(\eta-E_\alpha)P'_M(E_\alpha)$, where $P_M(x)=\Pi_{\alpha'=1}^{M}(x-E_{\alpha'})$ is the polynomial that has the unknowns E_α as its roots. One finds that

$$[2(s+Q)E_\alpha - 2Q\eta]P'_M(E_\alpha) + E_\alpha(\eta-E_\alpha)P''_M(E_\alpha) = 0, \tag{B2}$$

for $\alpha=1,\ldots,M$. Since this is a polynomial expression of order M, valid in M distinct points (assuming that none of the E_α coincide), one can identify the polynomial expression with a multiple of $P(x)$,

$$\begin{aligned}&[2(s+Q)x - 2Q\eta]P'_M(x) + x(\eta-x)P''_M(x) \\ &\quad = M[2(s+Q)-M+1]P_M(x), \quad \forall \quad x.\end{aligned}\tag{B3}$$

This equation can be transformed into the Jacobi equation in the variable y where $x=(\eta/2)(1+y)$. The solution is a Jacobi polynomial

$$P_M(x) \propto \mathcal{P}_M^{\alpha,\beta}(2x/\eta - 1) \tag{B4}$$

with parameters $\alpha=2Q/\eta-2Q-2s-1$ and $\beta=-2Q/\eta-1$.

Let us expand $P_M(x)=\Sigma_{i=0}^{M} p_{M,i}x^i$, where $p_{M,M}=1$. By equating orders of x^l in Eq. (B3), one obtains a recurrence relation that defines the coefficients $p_{M,i}$ completely

$$p_{M,i-1} = \eta\frac{(2Q+1-i)i}{[M+i-2-2(s+Q)](M+1-i)}p_{M,i},$$
$$\text{for } i=M,M-1,\ldots,1. \tag{B5}$$

If $2Q+1$ equals an integer value $N\leq M$, one sees that $P_M(x)$ has a factor x^N. This means that a singularity occurs in which N pairons will collapse at 0. Of particular interest are the cases $N=M$, where all pairons collapse to zero, and $N=0$, where no more singularities occur.

For multilevel systems, e.g., a system of l levels, the polynomial $P_M(x)$ is still well defined. Rather than a Jacobi-type equation, it now has to fulfill a *generalized Lamé differential equation* with negative residues,[42]

$$P_M''(x) + \left(\sum_{k=0}^{l}\frac{r_k}{x-\eta_k}\right)P_M'(x) - \frac{V_M(x)}{\prod_{k=0}^{l}(x-\eta_k)}P_M(x) = 0 \tag{B6}$$

with $r_0=-2Q$, $r_k=-2s_k$, and $\eta_0=0$. The solutions $P_M(x)$ are known as *Stieltjes polynomials*, while the polynomials $V_M(x)$ of order $l-1$ or less are known as *Van Vleck polynomials*. If all r_k were positive, i.e., all s_k and Q negative, which can occur for $su(1,1)$ representations (e.g., boson pairs), then the polynomials $P_M(x)$ would be orthogonal polynomials with respect to some weight function. The case of negative residues, $r_k<0$, is much less understood and a topic of ongoing research.[42]

APPENDIX C: CONTINUUM LIMIT OF THE INTEGRABLE p_x+ip_y MODEL

A full analysis of the continuum limit of the integrable p_x+ip_y has been presented in Refs. 22 and 43. We give here a brief overview of the procedure, that applies to the hyperbolic RG model in general, in order to maintain consistency with the other sections and to demonstrate that the transitions between the different regions in Fig. 1 are genuine phase transitions and not merely crossovers. The continuum limit of the RG equations [Eq. (17)] is based on the following scalings:

$$L,\ M\to\infty, \tag{C1}$$

$$M/L=\rho \quad \text{finite}, \tag{C2}$$

$$GL=g \quad \text{finite}, \tag{C3}$$

$$Q/L=q=\frac{1}{2g}-\frac{1}{2}+\rho, \tag{C4}$$

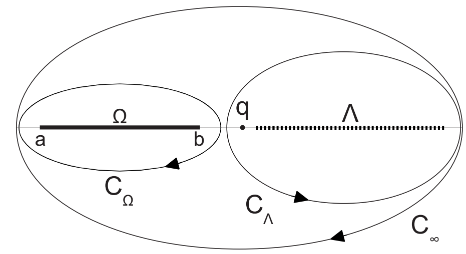

FIG. 12. Contours used to evaluate the continuum limit.

$$\frac{2}{L}\sum_k s_k f(\eta_k) \equiv \int_\Lambda \varrho(\eta)f(\eta)d\eta, \tag{C5}$$

$$\frac{1}{L}\sum_\alpha f(E_\alpha) \equiv \int_\Omega p(x)f(x)dx, \tag{C6}$$

where Λ is the support of the weighted level density $\varrho(\eta)$ and Ω the support of the pairon density $p(x)$. Their normalization is given by

$$\int_\Lambda \varrho(\eta)d\eta=1, \tag{C7}$$

$$\int_\Omega p(x)dx=\rho. \tag{C8}$$

The RG equations [Eq. (17)] take the following form in the continuum limit:

$$\frac{q}{x}+\frac{1}{2}\int_\Lambda\frac{\varrho(\eta)}{x-\eta}d\eta-\mathcal{P}\int_\Omega\frac{p(x')}{x-x'}dx'=0, \quad \forall\ x\in\Omega. \tag{C9}$$

The integral over x' is to be understood as a Cauchy principal value, $\mathcal{P}$. To solve this equation, we start from an electrostatic analogy that goes back to work of Stieltjes on orthogonal polynomials,[42,44] and has been applied in the present context by Gaudin[45] and was later elaborated in Refs. 28 and 46 for the rational model and in Refs. 22 and 43 for the hyperbolic model. One considers the pairons to represents M free charges with unit negative charge, positioned in the two-dimensional plane at coordinates given by the real and imaginary parts of pairon values E_α. Then Eq. (C9) represents the two-dimensional electrostatic force generated by the repulsion among the free charges, the attraction of a fixed charge density $\varrho(\eta)$ along the interval Λ, and the interaction with a central charge q located at the origin, derived from a potential $V(z)$ in the two-dimensional complex plane,

$$V(z)=-q\ln(|z|)-\frac{1}{2}\int_\Lambda\varrho(\eta)\ln(|z-\eta|)d\eta + \int_\Omega p(x')\ln(|z-x'|)dx'. \tag{C10}$$

Therefore, any particular solution of Eq. (C9) gives the equilibrium positions of the pairon density $p(x)$ in the two-dimensional plane. Note that q can change from attractive to repulsive depending on the filling ρ and on the coupling g. This change in sign is associated with a QPT whose interpretation is one of the main goals of this work. To find the unknown pairon density $p(x)$, we assume that it corresponds to a continuous charge distribution along a certain curve (or set of curves) Ω. The electric field $F(z)$ created by the charge q at the origin and the charge densities p (repulsive) and ϱ (attractive) will have a discontinuity across Ω given by

$$p(x) = \frac{F(x_+) - F(x_-)}{2\pi i}, \quad \text{for } x \in \Omega. \tag{C11}$$

This allows us to rewrite the Cauchy principal value integral over Ω as an integral along a clockwise contour C_Ω around Ω,

$$\mathcal{P}\int_\Omega \frac{p(x')}{x-x'}dx' = \frac{1}{2\pi i}\oint_{C_\Omega}\frac{F(z)}{x-z}dz. \tag{C12}$$

To model the discontinuity in $F(z)$ we propose the following ansatz:

$$F(z) = R_\Omega(z)\int_\Lambda \frac{\phi(\eta)}{z-\eta}d\eta, \tag{C13}$$

where $R_\Omega(z)$ is a function that explicitly takes into account a cut along Ω (Fig. 12). If Ω corresponds to a single segment with endpoints a and b, then one can take

$$R_{a-b}(z) = \sqrt{(z-a)(z-b)}. \tag{C14}$$

For more segments, $R_\Omega(z)$ has to be a higher order function, e.g.,

$$R_\Omega(z) = \prod_{i=1}^{n}\sqrt{(z-a_i)(z-b_i)}, \tag{C15}$$

where n is the number of segments. In general, one can write an asymptotic expansion for large z as

$$R_\Omega(z) = \sum_{i=0}^{+\infty} r_i z^{n-i}. \tag{C16}$$

Note that the total charge in the system is given by $\rho - q - 1/2 = -1/(2g)$. Therefore the asymptotic behavior of F is given by

$$F(z) = \frac{1}{2gz} + \mathcal{O}(z^{-2}), \quad \text{for } |z| \to \infty. \tag{C17}$$

This allows us to put constraints on the unknown function $\phi(z)$,

$$\int_\Lambda \phi(\eta)\eta^i d\eta = 0, \quad \text{for } i = 0, \ldots, n-1, \tag{C18}$$

$$\int_\Lambda \phi(\eta)\eta^n d\eta = \frac{1}{2g}. \tag{C19}$$

Now we can rewrite Eq. (C12) by deforming the contour around Ω into a contour C_Λ around Λ plus a contour C_∞ around the point at infinity

$$\begin{aligned}\mathcal{P}\int_\Omega \frac{p(x')}{x-x'}dx' &= \frac{1}{2\pi i}\oint_{C_\Omega}\frac{R_\Omega(z)}{x-z}\int_\Lambda \frac{\phi(\eta)}{z-\eta}d\eta dz \\ &= \frac{1}{2\pi i}\int_\Lambda \phi(\eta)\oint_{C_\Lambda}\frac{R_\Omega(z)}{(z-\eta)(x-z)}dz d\eta \\ &\quad + \frac{1}{2\pi i}\int_\Lambda \phi(\eta)\oint_{C_\infty}\frac{R_\Omega(z)}{(z-\eta)(x-z)}dz d\eta \\ &= \int_\Lambda \frac{\phi(\eta)R_\Omega(\eta)}{x-\eta}d\eta,\end{aligned} \tag{C20}$$

where the integral along C_∞ vanishes because of Eq. (C18) as can be seen in the following expansion:

$$\begin{aligned}&\int_\Lambda \phi(\eta)\oint_{C_\infty}\frac{R_\Omega(z)}{(z-\eta)(x-z)}dz d\eta \\ &= -\int_\Lambda \phi(\eta)\oint_{C_\infty}\frac{\sum_{j=0}^{+\infty} r_j z^{n-j-2}}{(1-\eta/z)(1-x/z)}dz d\eta \\ &= -\sum_{j,k,l=0}^{+\infty} x^l r_j \int_\Lambda \phi(\eta)\eta^k d\eta \oint_{C_\infty} z^{n-j-k-l-2}dz \\ &= 2\pi i \sum_{j=0,k=0,l=0}^{+\infty} x^l r_j \delta_{k,n-1-j-l}\int_\Lambda \phi(\eta)\eta^k d\eta = 0\end{aligned} \tag{C21}$$

because only terms with $k < n$ are allowed by the Kronecker delta. Comparing Eq. (C20) with Eq. (C9), we find that the solution is given by

$$\phi(\eta) = \frac{q\delta(\eta) + \frac{1}{2}\varrho(\eta)}{R_\Omega(\eta)}. \tag{C22}$$

The segments of Ω correspond to equipotential curves in the complex plane, determined by

$$\text{Re}\int_{a_n}^{z_n} F(z)dz = 0. \tag{C23}$$

The energy density is given by $\varepsilon = E/L$ and can be evaluated as

$$\begin{aligned}\varepsilon &= \langle \nu|H_h|\nu\rangle/L + \int_\Omega xp(x)dx \\ &= -\frac{1}{2}\int_\Lambda \eta\varrho(\eta)d\eta + \frac{1}{2\pi i}\oint_{C_\Omega} zR_\Omega(z)\int_\Lambda \frac{\phi(\eta)}{z-\eta}d\eta dz \\ &= -\frac{1}{2}\int_\Lambda \eta\varrho(\eta)d\eta + \frac{1}{2\pi i}\oint_{C_\Lambda} zR_\Omega(z)\int_\Lambda \frac{\phi(\eta)}{z-\eta}d\eta dz \\ &\quad + \frac{1}{2\pi i}\oint_{C_\infty} zR_\Omega(z)\int_\Lambda \frac{\phi(\eta)}{z-\eta}d\eta dz \\ &= -\frac{1}{2}\int_\Lambda \eta\varrho(\eta)d\eta + \frac{1}{2}\int_\Lambda \eta\varrho(\eta)d\eta\end{aligned}$$

$$+\frac{1}{2\pi i}\sum_{j,k=0}^{\infty} r_j \int_{\Lambda} \phi(\eta)\eta^k d\eta \oint_{C_\infty} z^{n-j-k} dz$$

$$=-\frac{1}{2}\int_{\Lambda} \varrho(\eta)\frac{\eta^{n+1}}{R_\Omega(\eta)}d\eta + \sum_{i=1}^{n}\frac{(a_i+b_i)}{4g}. \quad \text{(C24)}$$

Let us analyze in particular the case of a single segment, i.e. $n=1$. Eqs. (C18) and (C19) reduce to

$$\frac{\sqrt{ab}}{2}\int_{\Lambda}\frac{\varrho(\eta)}{\sqrt{(\eta-a)(\eta-b)}}d\eta = -q = \frac{1}{2}-\frac{1}{2g}-\rho, \quad \text{(C25)}$$

$$\int_{\Lambda}\frac{\varrho(\eta)\eta}{\sqrt{(\eta-a)(\eta-b)}}d\eta = \frac{1}{g}. \quad \text{(C26)}$$

It is interesting to compare this to the result of a mean-field theory for the ground state (see Appendix D) based on a grand potential $H_h-\mu S^z$, with chemical potential μ and a pairing field $\Delta = G\Sigma_k\sqrt{\eta_k}\langle S_k^-\rangle$. One obtains the same expressions as in Eqs. (C25) and (C26), provided that one equates

$$\sqrt{(\eta-a)(\eta-b)} = \sqrt{(\eta-2\mu)^2+4\eta\Delta^2}, \quad \text{(C27)}$$

which means that one can identify

$$a+b = 4(\mu-\Delta^2), \quad ab = 4\mu^2, \quad \text{(C28)}$$

$$a-b = \pm 4\Delta\sqrt{\Delta^2-2\mu}, \quad \text{(C29)}$$

$$\mu = \pm\frac{\sqrt{ab}}{2}, \quad \Delta^2 = \pm\frac{\sqrt{ab}}{2}-\frac{a+b}{4}. \quad \text{(C30)}$$

Again one can distinguish the three regions in the quantum phase diagram: *weak-coupling BCS*. $0<\frac{\Delta^2}{2}<\mu$, and a and b complex. The pairons form an arc in the complex plane. *Weak pairing at intermediate coupling*. $0<\mu<\frac{\Delta^2}{2}$, and a and b real and negative. The distribution of pairons along the negative real axis between a and b has to be supplemented with two arcs in the complex plane that close around the origin, touching the real negative axis in a, and a segment of real positive pairons between the origin and the point where the arcs touch the positive real axis. *Strong pairing*. $\mu<0$, and a and b real and negative. All pairons fall in the segment on the negative real axis between a and b.

For $n=1$ one can further elaborate Eq. (C24) for the energy

$$\varepsilon = \frac{\mu}{g}-\frac{\Delta^2}{g}-\frac{1}{2}\int_{\Lambda}\varrho(\eta)\frac{\eta^2}{\sqrt{(\eta-2\mu)^2+4\eta\Delta^2}}d\eta$$

$$=\mu(2\rho-1)+\frac{\Delta^2}{g}-\Theta(\mu,\Delta^2), \quad \text{(C31)}$$

where we have defined

$$\Theta(\mu,\Delta^2) = \frac{1}{2}\int_{\Lambda}\varrho(\eta)\sqrt{(\eta-2\mu)^2+4\eta\Delta^2}d\eta. \quad \text{(C32)}$$

We can formally express Eqs. (C25) and (C26) as

$$\frac{\partial\Theta}{\partial\mu}(\mu,\Delta^2) = 2\rho-1, \quad \frac{\partial\Theta}{\partial\Delta^2}(\mu,\Delta^2) = \frac{1}{g}. \quad \text{(C33)}$$

Substituting these conditions into Eq. (C31), we see that they guarantee that $\varepsilon(\mu,\Delta^2)$ reaches an extremum at the corresponding values of μ and Δ^2, which coincides with the mean-field theory of Appendix D.

Note that the pairon distribution does not depend on the details of the representation for the $su(2)$ operators $\mathbf{S}_k$. The only model factor that enters into the equations is the weighted level density $\varrho(\eta)$, which corresponds to the distribution of s_k in the vacuum state $|\nu\rangle$. The fact that ε, ρ, and g all depend on $\Theta(\mu,\Delta^2)$ means that a QPT will occur only if $\Theta(\mu,\Delta^2)$ displays a singularity in one of its derivatives. From Eq. (C32) one can infer that this will be the case if the argument of the square root vanishes, which happens at $\mu=0$ if $\eta=0$ is included in the domain Λ.

APPENDIX D: MEAN-FIELD THEORY OF THE HYPERBOLIC RICHARDSON-GAUDIN MODEL

Mean-field theories for separable interactions have been discussed before in the context of p_x+ip_y pairing models.[16,18] Here we present a more general derivation applicable to all exactly solvable models derived from the hyperbolic RG model, the p_x+ip_y model representing a particular case. Our mean-field theory for the Hamiltonian H_h from Eq. (16) is based on a variational wave function

$$|\theta\rangle = e^{\Sigma_k\theta_k S_k^+}|\nu\rangle. \quad \text{(D1)}$$

For fermions, the mean-field theory is often presented in terms of a double set of complex parameters $v_k/u_k=\theta_k$, with the condition that $|u_k|^2+|v_k|^2=1$. These parameters can be related to θ_k as

$$u_k = \frac{1}{\sqrt{1+|\theta_k|^2}}, \quad v_k = \frac{\theta_k}{\sqrt{1+|\theta_k|^2}}, \quad \text{(D2)}$$

Let us denote normalized expectation values as $\langle\ldots\rangle$. From the normalization condition

$$\langle\theta|\theta\rangle = \prod_k (1+|\theta_k|^2)^{2s_k}, \quad S_k^z|\nu\rangle = -s_k|\nu\rangle, \quad \text{(D3)}$$

one easily finds the normalized expectation values for the basic operators of the algebra

$$\langle S_k^z\rangle = -s_k\frac{1-|\theta_k|^2}{1+|\theta_k|^2}, \quad \langle S_k^-\rangle = 2s_k\frac{\theta_k}{1+|\theta_k|^2}. \quad \text{(D4)}$$

Furthermore, one can show that

$$\langle S_k^+S_{k'}^-\rangle = \langle S_k^+\rangle\langle S_{k'}^-\rangle + \delta_{kk'}\frac{(s_k+\langle S_k^z\rangle)^2}{2s_k}. \quad \text{(D5)}$$

This allows us to write the mean-field expectation value for H_h as

$$\langle H_h\rangle = \sum_k \eta_k \langle S_k^z\rangle - G\sum_{k,k'} \sqrt{\eta_k\eta_{k'}}\langle S_k^+\rangle\langle S_{k'}^-\rangle - G\sum_k \eta_k \frac{(s_k+\langle S_k^z\rangle)^2}{2s_k}. \quad \text{(D6)}$$

To derive the mean-field equations, we will vary the following expression:

$$\langle\theta|H_h|\theta\rangle - 2\mu\langle\theta|S^z|\theta\rangle - E_{\mathrm{mf}}\langle\theta|\theta\rangle, \quad \text{(D7)}$$

where μ is a Lagrange multiplier that fixes $\langle S^z\rangle$ and represents the chemical potential in particle (fermion or boson) representations of the model while E_{mf} is needed to fix the normalization. By varying Eq. (D7) with respect to $\langle\theta|$ we obtain the mean-field equation

$$H_{\mathrm{mf}}|\theta\rangle = E_{\mathrm{mf}}|\theta\rangle \quad \text{(D8)}$$

with

$$H_{\mathrm{mf}} = 2\sum_k \xi_k S_k^z - \sum_k \sqrt{\eta_k}(\Delta S_k^+ + \Delta^* S_k^-), \quad \text{(D9)}$$

$$\xi_k = \left(\frac{1}{2} - G\frac{s_k+\langle S_k^z\rangle}{2s_k}\right)\eta_k - \mu, \quad \text{(D10)}$$

$$\Delta = G\sum_k \sqrt{\eta_k}\langle S_k^-\rangle. \quad \text{(D11)}$$

To check whether the ansatz of Eq. (D1) is indeed an eigenstate of H_{mf}, we evaluate

$$\begin{aligned} H_{\mathrm{mf}}|\theta\rangle &= e^{\sum_k\theta_k S_k^+}e^{-\sum_k\theta_k S_k^+}H_{\mathrm{mf}}e^{\sum_k\theta_k S_k^+}|\nu\rangle \\ &= e^{\sum_k\theta_k S_k^+}\Bigg(2\sum_k[\xi_k+\theta_k\sqrt{\eta_k}\Delta^*]S_k^z \\ &\quad + \sum_k[(\theta_k^2\Delta^*-\Delta)\sqrt{\eta_k}+2\theta_k\xi_k]S_k^+ - \sum_k\sqrt{\eta_k}\Delta^* S_k^-\Bigg)|\nu\rangle. \end{aligned} \quad \text{(D12)}$$

One sees that $|\theta\rangle$ is an eigenstate provided that

$$(\theta_k^2\Delta^*-\Delta)\sqrt{\eta_k}+2\theta_k\xi_k = 0. \quad \text{(D13)}$$

The corresponding eigenvalue of H_{mf} is given by

$$E_{\mathrm{mf}} = -2\sum_k s_k[\xi_k+\theta_k\sqrt{\eta_k}\Delta^*]. \quad \text{(D14)}$$

θ_k must have the same phase as Δ, which we can absorb in the definition of the operator $\mathbf{S}_k$, so we can take Δ and θ_k to be real without loss of generality. One finds that the ground-state solution of Eq. (D13) is given by

$$\theta_k = \frac{\sqrt{\xi_k^2+\eta_k\Delta^2}-\xi_k}{\sqrt{\eta_k}\Delta}. \quad \text{(D15)}$$

Then, the mean-field eigenvalue becomes

$$E_{\mathrm{mf}} = -2\sum_k s_k\sqrt{\xi_k^2+\eta_k\Delta^2} \quad \text{(D16)}$$

and the expectation values become

$$\langle S_k^z\rangle = -s_k\frac{\xi_k}{\sqrt{\xi_k^2+\eta_k\Delta^2}}, \quad \langle S_k^-\rangle = s_k\frac{\sqrt{\eta_k}\Delta}{\sqrt{\xi_k^2+\eta_k\Delta^2}}, \quad \text{(D17)}$$

$$\langle H_h\rangle = -\sum_k s_k\frac{\xi_k\eta_k}{\sqrt{\xi_k^2+\eta_k\Delta^2}} - \frac{\Delta^2}{G} - G\sum_k\frac{\eta_k s_k}{2}\left(1-\frac{\xi_k}{\sqrt{\xi_k^2+\eta_k\Delta^2}}\right)^2. \quad \text{(D18)}$$

In the particle representation of Eq. (21), the occupation probabilities are given by

$$\langle c_k^\dagger c_k\rangle = \frac{1}{2} - \frac{\langle S_k^z\rangle}{2s_k} = \frac{1}{2} - \frac{\xi_k}{2\sqrt{\xi_k^2+\eta_k\Delta^2}}. \quad \text{(D19)}$$

Self-consistency with the definition of Δ in Eq. (D11) gives us the gap equation

$$\sum_k s_k\frac{\eta_k}{\sqrt{\xi_k^2+\eta_k\Delta^2}} = \frac{1}{G} \quad \text{(D20)}$$

while fixing the expectation value of S^z gives us the number equation

$$-\sum_k s_k\frac{\xi_k}{\sqrt{\xi_k^2+\eta_k\Delta^2}} = M - L/2. \quad \text{(D21)}$$

In the thermodynamic limit $L\to\infty$, with $g=GL$ finite. The expression for ξ_k simplifies to

$$\xi_k = \eta_k/2 - \mu. \quad \text{(D22)}$$

Adding 1/2 times Eq. (D20) to Eq. (D21) allows us to rewrite the number equation as

$$\frac{1}{L}\sum_k s_k\frac{\mu}{\sqrt{\xi_k^2+\eta_k\Delta^2}} = \frac{1}{2g} - 1/2 + \rho. \quad \text{(D23)}$$

We see that $\mu=0$ occurs at $g^{-1}=1-2\rho$, i.e. *special case (i)* from Sec. II B. Another interesting situation occurs when $\mu=\frac{\Delta^2}{2}$ because then one has that $\sqrt{\xi_k^2+\eta_k\Delta^2}=|\eta_k/2+\mu|$ and consequently $\theta_k=\Delta/k$. By adding 1/2 times Eq. (D20) to Eq. (D23) for this case, one obtains (assuming all $\eta_k>0$) that $g^{-1}=1-\rho$, i.e., *special case (ii)* from Sec. II B.

APPENDIX E: HIGHER ORDER DERIVATIVES IN THE THERMODYNAMIC LIMIT

From Eq. (38) we notice that g^{-1} and 2ρ are conjugate quantities to Δ^2 and μ,

$$\frac{\partial\varepsilon}{\partial(g^{-1})} = \Delta^2, \quad \frac{\partial\varepsilon}{\partial(2\rho)} = \mu. \quad \text{(E1)}$$

We can thus obtain the Jacobian matrix J with respect to Δ^2 and μ, after Eqs. (34) and (35),

$$J = \begin{pmatrix} \frac{\partial(g^{-1})}{\partial(\Delta^2)} & \frac{\partial(g^{-1})}{\partial\mu} \\ \frac{\partial(2\rho)}{\partial(\Delta^2)} & \frac{\partial(2\rho)}{\partial\mu} \end{pmatrix}, \quad \text{(E2)}$$

whose inverse

$$J^{-1} = \begin{pmatrix} \frac{\partial(\Delta^2)}{\partial(g^{-1})} & \frac{\partial(\Delta^2)}{\partial(2\rho)} \\ \frac{\partial\mu}{\partial(g^{-1})} & \frac{\partial\mu}{\partial(2\rho)} \end{pmatrix} \tag{E3}$$

represents the Hessian of ε with respect to g^{-1} and 2ρ because of Eq. (E1). If the matrix elements of J^{-1} are continuous and its determinant is nonzero over the whole parameter space, then the second-order derivatives of ε are continuous. For instance, the second-order derivative of ε with respect to g^{-1}, keeping ρ constant, is

$$\frac{\partial^2\varepsilon}{(\partial g^{-1})^2} = \frac{\partial(\Delta^2)}{\partial(g^{-1})} = \frac{\partial(2\rho)}{\partial\mu}\det(J^{-1}) \tag{E4}$$

and the second-order derivative with respect to g can then be obtained as

$$\frac{\partial^2\varepsilon}{(\partial g)^2} = \frac{2}{g^3}\frac{\partial\varepsilon}{\partial(g^{-1})} + \frac{1}{g^4}\frac{\partial^2\varepsilon}{(\partial g^{-1})^2}$$

$$= \frac{2}{g^3}\Delta^2 + \frac{1}{g^4}\frac{\partial(2\rho)}{\partial\mu}\det(J^{-1}). \tag{E5}$$

To obtain a compact notation for the derivatives, we define the following quantities:

$$V = \sqrt{(\omega-\mu)^2 + 2\omega\Delta^2}, \tag{E6}$$

$$F = \omega - \mu + \Delta^2 + V, \tag{E7}$$

$$f = \Delta^2 - \mu + |\mu|, \tag{E8}$$

$$\zeta = \frac{g^{-1} + 2\rho - 1}{\mu} = \frac{1}{\omega}\ln\left(\frac{F}{f}\right). \tag{E9}$$

Then we can derive

$$\frac{\partial(g^{-1})}{\partial(\Delta^2)} = -\zeta - \frac{|\mu|}{\omega f} + \frac{(\omega+V)^2}{\omega V F}, \tag{E10}$$

$$\frac{\partial(g^{-1})}{\partial\mu} = \frac{\partial(2\rho)}{\partial(\Delta^2)} = \zeta - \frac{\mu - |\mu|}{\omega f} - \frac{(\omega+V)(\omega+V-\mu)}{\omega V F}, \tag{E11}$$

$$\frac{\partial(2\rho)}{\partial\mu} = 2\frac{\mu - |\mu|}{\omega f} + \frac{(\omega+V-\mu)^2}{\omega V F}. \tag{E12}$$

By combining these results one finds that

$$\det(J) = \frac{2\zeta}{V} - \zeta^2 - |\mu|\frac{(\omega+V-|\mu|)^2}{\omega^2 V f F}. \tag{E13}$$

For $g \neq 0$ we know that $\Delta^2 > 0$. One easily verifies that then also $V > 0$, $F > f > 0$. The quantity ζ remains finite and continuous when μ crosses 0, as can be seen from the right-hand side of Eq. (E9). Hence the only singularities in the derivative of Eq. (E5) can come from a zero in the determinant of J. By inspection one finds that $\det(J) < 0$ for all finite values of μ and Δ^2, even though there is a cusp at $\mu=0$ due to the absolute value $|\mu|$ that appears in Eqs. (E8) and (E13). For $\mu \to 0$, the condition $\det(J)=0$ is satisfied if and only if

$$V\zeta = 2$$

$$\Updownarrow$$

$$\frac{V}{\omega}\ln\left(\frac{F}{f}\right) = 2$$

$$\Updownarrow$$

$$\frac{V+\omega}{V-\omega} = e^{2\omega/V}$$

$$\Updownarrow$$

$$\frac{\omega}{V} = \tanh\left(\frac{\omega}{V}\right)$$

$$\Updownarrow$$

$$\Delta^2 = \infty. \tag{E14}$$

However, Δ^2 is finite for any finite value of g implying that there is no discontinuity in the second-order derivative of the energy at $\mu=0$, where the quantum phase transition occurs.

The third-order derivatives of ε can be written as combinations of Eqs. (E10)–(E13) and their derivatives. Because of the cusp in $\det(J)$ at $\mu=0$ one can expect a discontinuity in the third-order derivatives at the phase-transition line, as indicated in Fig. 9.

*rombouts@iem.cfmac.csic.es

[1] S. Giorgini, L. P. Pitaevskii, and S. Stringari, Rev. Mod. Phys. **80**, 1215 (2008).
[2] A. J. Leggett, Rev. Mod. Phys. **47**, 331 (1975).
[3] D. J. Dean and M. Hjorth-Jensen, Rev. Mod. Phys. **75**, 607 (2003).
[4] J. Bardeen, L. N. Cooper, and J. R. Schrieffer, Phys. Rev. **108**, 1175 (1957).
[5] A. J. Leggett, *Modern Trends in the Theory of Condensed Matter* (Springer Verlag, Berlin, 1980).
[6] C. A. Regal, C. Ticknor, J. L. Bohn, and D. S. Jin, Phys. Rev. Lett. **90**, 053201 (2003).
[7] J. Zhang, E. G. M. van Kempen, T. Bourdel, L. Khaykovich, J. Cubizolles, F. Chevy, M. Teichmann, L. Tarruell, S. J. J. M. F.

Kokkelmans, and C. Salomon, Phys. Rev. A **70**, 030702 (2004).
[8] C.-H. Cheng and S.-K. Yip, Phys. Rev. Lett. **95**, 070404 (2005).
[9] C. Zhang, S. Tewari, R. M. Lutchyn, and S. Das Sarma, Phys. Rev. Lett. **101**, 160401 (2008).
[10] Y. Nishida, Ann. Phys. **324**, 897 (2009).
[11] N. R. Cooper and G. V. Shlyapnikov, Phys. Rev. Lett. **103**, 155302 (2009).
[12] P. Massignan, A. Sanpera, and M. Lewenstein, Phys. Rev. A **81**, 031607(R) (2010).
[13] J. Xia, Y. Maeno, P. T. Beyersdorf, M. M. Fejer, and A. Kapitulnik, Phys. Rev. Lett. **97**, 167002 (2006).
[14] N. Read and D. Green, Phys. Rev. B **61**, 10267 (2000).
[15] V. Gurarie, L. Radzihovsky, and A. V. Andreev, Phys. Rev. Lett. **94**, 230403 (2005).
[16] S. S. Botelho and C. A. R. Sá de Melo, J. Low Temp. Phys. **140**, 409 (2005).
[17] M. Iskin and C. A. R. Sá de Melo, Phys. Rev. Lett. **96**, 040402 (2006).
[18] M. I. Ibañez, J. Links, G. Sierra, and S. Y. Zhao, Phys. Rev. B **79**, 180501(R) (2009).
[19] Interestingly, in Ref. 14 the motivation to study the weak-pairing phase was to relate its properties to the Moore-Read state supposed to represent a $\nu=5/2$ fractional quantum Hall liquid. The Moore-Read state in the coordinate representation is a Pfaffian which can be asymptotically related to the weak-pairing wave function (in the limit of large pair separation).
[20] G. E. Volovik, Sov. Phys. JETP **67**, 1804 (1988).
[21] C. Nayak, S. H. Simon, A. Stern, M. Freedman, and S. Das Sarma, Rev. Mod. Phys. **80**, 1083 (2008).
[22] C. Dunning, M. Ibanez, J. Links, G. Sierra, and S.-Y. Zhao, J. Stat. Mech.: Theory Exp. (2010) P08025.
[23] G. Moore and N. Read, Nucl. Phys. B **360**, 362 (1991).
[24] L. Amico, A. Di Lorenzo, and A. Osterloh, Phys. Rev. Lett. **86**, 5759 (2001).
[25] J. Dukelsky, C. Esebbag, and P. Schuck, Phys. Rev. Lett. **87**, 066403 (2001).
[26] G. Ortiz, R. Somma, J. Dukelsky, and S. Rombouts, Nucl. Phys. B **707**, 421 (2005).
[27] M. Gaudin, J. Phys. (France) **37**, 1087 (1976).
[28] J. Dukelsky, C. Esebbag, and S. Pittel, Phys. Rev. Lett. **88**, 062501 (2002).
[29] C. D. Batista and G. Ortiz, Adv. Phys. **53**, 1 (2004).
[30] S. Rombouts, D. Van Neck, and J. Dukelsky, Phys. Rev. C **69**, 061303 (2004).
[31] F. Domínguez, C. Esebbag, and J. Dukelsky, J. Phys. A **39**, 11349 (2006).
[32] R. W. Richardson, Phys. Rev. **141**, 949 (1966).
[33] K. Levenberg, Q. Appl. Math. **2**, 164 (1944); D. Marquardt, SIAM J. Appl. Math. **11**, 431 (1963).
[34] See supplementary material at http://link.aps.org/supplemental/10.1103/PhysRevB.82.224510 for a video of the pairon evolution as a function of g for this system (126 pairons with $L=504$).
[35] C. N. Yang, Rev. Mod. Phys. **34**, 694 (1962).
[36] A. Faribault, P. Calabrese, and J. S. Caux, Phys. Rev. B **77**, 064503 (2008).
[37] S. Rombouts, D. Van Neck, K. Peirs, and L. Pollet, Mod. Phys. Lett. A **17**, 1899 (2002).
[38] G. Ortiz and J. Dukelsky, Phys. Rev. A **72**, 043611 (2005); *Condensed Matter Theories*, edited by H. Akai, A. Hosaka, H. Toki, and F. B. Malik (Nova Science, Huntington, New York, 2007), Vol. 21.
[39] T. Rom, T. Best, D. van Oosten, U. Schneider, S. Folling, B. Paredes, and I. Bloch, Nature (London) **444**, 733 (2006).
[40] J. Dukelsky, G. Ortiz, and S. M. A. Rombouts, Int. J. Mod. Phys. B **20**, 5179 (2006).
[41] B. S. Shastry and A. Dhar, J. Phys. A **34**, 6197 (2001).
[42] F. Marcellán, A. Martínez-Finkelshtein, and P. Martínez-González, J. Comput. Appl. Math. **207**, 258 (2007).
[43] L. Amico, A. Di Lorenzo, A. Mastellone, A. Osterloh, and R. Raimondi, Ann. Phys. **299**, 228 (2002), the equations presented in this reference can be related to our results through the transformation $z_\alpha=(E_\alpha^2-1)/(E_\alpha^2+1)$.
[44] D. K. Dimitrov and W. Van Assche, Proc. Am. Math. Soc. **128**, 3621 (2000).
[45] M. Gaudin, *Travaux de Michel Gaudin: Modeèles exactement résolus* (Les Editions de Physique, Les Ulis, 1995).
[46] J. M. Román, G. Sierra, and J. Dukelsky, Nucl. Phys. B **634**, 483 (2002).